Biophysical Chemistry 205 (2015) 51–65

Contents lists available at ScienceDirect

Biophysical Chemistry

journal homepage: http://www.elsevier.com/locate/biophyschem

# Intrinsic thermodynamics of 4-substituted-2,3,5,6-tetrafluorobenzenesulfonamide binding to carbonic anhydrases by isothermal titration calorimetry

Asta Zubrienė [a,*], Joana Smirnovienė [a], Alexey Smirnov [a], Vaida Morkūnaitė [a], Vilma Michailovienė [a], Jelena Jachno [a], Vaida Juozapaitienė [a], Povilas Norvaišas [a], Elena Manakova [b], Saulius Gražulis [b], Daumantas Matulis [a]

[a] Department of Biothermodynamics and Drug Design, Institute of Biotechnology, Vilnius University, Graičiūno 8, Vilnius LT-02241, Lithuania
[b] Department of Protein–DNA Interactions, Institute of Biotechnology, Vilnius University, Graičiūno 8, Vilnius LT-02241, Lithuania

## HIGHLIGHTS

- Compounds bind CA I with $K_d = 2$ pM, nearly tightest for any protein–ligand binding.
- Fluorination has a large effect on the observed but not the intrinsic affinities.
- Compound binding was enthalpy-driven to CAs I, II, VII and XIII.

## GRAPHICAL ABSTRACT

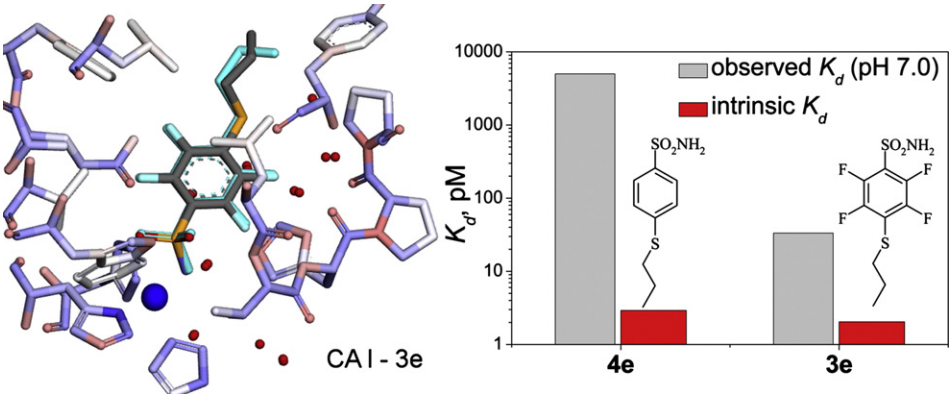


## ARTICLE INFO

*Article history:*
Received 28 April 2015
Received in revised form 21 May 2015
Accepted 21 May 2015
Available online 6 June 2015

*Keywords:*
Carbonic anhydrase inhibitors
Isothermal titration calorimetry
X-ray crystallography
Intrinsic thermodynamics of binding
Structure–thermodynamics relationships

## ABSTRACT

*Para* substituted tetrafluorobenzenesulfonamides bind to carbonic anhydrases (CAs) extremely tightly and exhibit some of the strongest known protein–small ligand interactions, reaching an intrinsic affinity of 2 pM as determined by displacement isothermal titration calorimetry (ITC). The enthalpy and entropy of binding to five CA isoforms were measured by ITC in two buffers of different protonation enthalpies. The p$K_a$ values of compound sulfonamide groups were measured potentiometrically and spectrophotometrically, and enthalpies of protonation were measured by ITC in order to evaluate the proton linkage contributions to the observed binding thermodynamics. Intrinsic means the affinity of a sulfonamide anion for the Zn bound water form of CAs. Fluorination of the benzene ring significantly enhanced the observed affinities as it increased the fraction of deprotonated ligand while having little impact on intrinsic affinities. Intrinsic enthalpy contributions to the binding affinity were dominant over entropy and were more exothermic for CA I than for other CA isoforms. Thermodynamic measurements together with the X-ray crystallographic structures of protein–ligand complexes enabled analysis of structure–activity relationships in this enzyme ligand system.



* Corresponding author at: Graičiūno 8, Vilnius LT-02241, Lithuania.
*E-mail addresses:* astzu@ibt.lt, asta.zubriene@bti.vu.lt (A. Zubrienė).

http://dx.doi.org/10.1016/j.bpc.2015.05.009
0301-4622/

## 1. Introduction

Protein–ligand interactions are one of the main objects of study in protein biophysical chemistry. Molecular forces and underlying reasons that distinguish marginal from high affinity or selectivity as well as the impact of water solvent are not well understood. Thermodynamic characterization of protein–ligand interaction can be an important step in drug discovery and optimization of a hit to lead development. Deep understanding of the energetic forces driving the binding interaction provides valuable information for further drug development. To achieve high-affinity binding both favorable entropic and enthalpic contributions are desired [1]. However, changes in the structure of ligand usually lead to compensating changes in the enthalpy and entropy of binding resulting in little or no improvement of binding affinity [2–6] thus making it a difficult step in drug development [7].

The protein–ligand binding process is governed by non-covalent interactions such as electrostatic, hydrogen bonding, metal coordination, hydrophobic, van der Waals interactions, halogen bonds, solvation effects and dynamic structural changes of interacting ligand and protein [8–11]. The enthalpic and entropic contributions to the Gibbs free energy reflect the specificity and strength of these interactions between both partners. Water molecules at or close to the interface could play a crucial role in the binding process [12–17], modulating enthalpy/entropy profile and thus binding affinity.

Two kinds of structure–activity relationships can be distinguished, first — the correlation of ligand chemical structure with the binding thermodynamics and second — the correlation of binding thermodynamics with the 3D structure of the protein–ligand complex. The correlation of thermodynamics of binding with the structural properties of protein–ligand crystallographic complexes can give valuable information about the nature of recognition phenomena especially when congeneric compound series are investigated [16]. However, prior to factorization of the Gibbs free energy of binding into enthalpic and entropic contributions, knowledge about the protonation/deprotonation of the interacting molecules is of utmost importance. If such proton linkage is observed, the observed binding parameters, enthalpy and binding constant, at a given pH may not reflect the intrinsic binding parameters and result in misinterpretation of the data [18,19]. By intrinsic we here mean the binding thermodynamics where binding-linked protonation reactions were subtracted from the observed reactions.

In the present study, we investigated the binding of tetrafluorobenzenesulfonamides as carbonic anhydrase (CA) inhibitors which were substituted at the *para* position by different, mainly hydrophobic, chemical groups. CA is a metalloenzyme that catalyzes reversible carbon dioxide hydration and participates in the regulation of acid–base balance and ion transport in all human tissues and organs. There are 15 different α-CA isoforms in humans, 12 possess catalytic activity, whereas CA VIII, CA X, and CA XI are inactive [20,21]. The enhanced activity or expression of different CAs is associated with various diseases such as glaucoma, epilepsy and cancer [21]. Although more than 30 sulfonamides are used clinically for the treatment of these diseases, there is a need for more selective compounds [22]. Therefore numerous inhibitors are being synthesized to achieve desirable selectivity. All catalytically active human α-CAs have highly conserved sequence and three-dimensional structure [23–25], therefore the rational design of selective and tightly binding CA inhibitors is not an easy task.

CA has a single active site with a zinc atom, which is coordinated by three conserved histidine residues (His94, His96 and His119) and a water molecule. In some isoforms His64 acts as a proton shuttle and participates in the conversion of the Zn bound water molecule to the hydroxide ion before $CO_2$ hydration reaction. The mechanism of inhibitor binding in the active site to Zn is clearly determined. All inhibitors bearing the sulfonamide group bind to the catalytic Zn atom in their ionized (deprotonated) form [26]. A large number of crystal structures with inhibitors bound to most CA isoforms have been determined. Despite a large amount of kinetic and biophysical data, there are only a small number of comprehensive thermodynamic studies of this system, describing the driving forces determining binding affinity.

Human CA II is the most extensively studied protein among 15 CA isoforms and its structure is characterized in the greatest detail by X-ray and neutron diffraction [26,27]. Whitesides and coworkers used CA II as a model protein for the study of hydrophobic effect and related phenomena such as enthalpy–entropy compensation in protein–ligand interactions [14,28–30]. In the study of a series of heterocyclic aromatic sulfonamides binding to CA II [30] they found that the binding affinity increases as the ligand nonpolar surface increases and was enthalpically driven. Their results revealed the importance of solvent water to the binding energetics. The study of benzothiazole sulfonamides with different patterns of fluorination confirmed the same hypothesis that the structure of the networks of hydrogen-bonded water molecules determines the enthalpy/entropy compensation [14,28].

Recently we have described the synthesis of series 4-substituted-2,3,5,6-tetrafluorobenezenesulfonamides as well as nonfluorinated 4-substituted benzenesulfonamides and measured their binding affinities to CA I, CA II, CA VII, CA XII and CA XIII by the fluorescent thermal shift assay (FTSA) [31]. Despite a simple chemical structure of most of the fluorinated compounds, they exhibited implausibly strong (up to single-digit picomolar) binding affinity toward tested CAs and showed selectivity toward CA I. The motivation of this manuscript was the thorough understanding of tight binding of fluorinated compounds to CAs by considering entropic and enthalpic contributions to the binding process. Intrinsic thermodynamic parameters independent of experimental conditions (pH and enthalpy of buffer ionization) and the properties of sulfonamide and protein ($pK_a$ and enthalpy of ionization) were determined and correlated with high-resolution protein–ligand crystal structures. The influence of the nature of the *para* substituents on fluorinated

**Table 1**
Thermodynamic parameters of the protonation of inhibitor sulfonamide group are listed for all compounds. The p$K_a$ were determined spectrophotometrically or by potentiometric titration (in the brackets) while the enthalpies of protonation were determined by ITC or by the van't Hoff relationship (in the brackets) of the p$K_a$ dependence on temperature.

| No | p$K_a$, at 37 °C | $\Delta_{b\_proton}G$, kJ/mol | $\Delta_{b\_proton}H$, kJ/mol | $-T\Delta_{b\_proton}S$, kJ/mol |
|---|---|---|---|---|
| **1** | 8.21 (8.30) | −48.8 | −25.9 | −22.8 |
| **2** | 8.12 (8.00) | −48.2 | −26.4 | −21.9 |
| **3a** | 8.84 | −52.5 | −29.0 | −23.5 |
| **3c** | 8.14 | −48.3 | −26.4 (−21.0) | −22.0 |
| **3d** | 7.28 | −43.2 | −23.8 | −19.4 |
| **3e** | 8.15 (8.00) | −48.4 | −26.4 (−25.6) | −22.0 |
| **3f** | 8.14 | −48.3 | −26.4 | −22.0 |
| **3g** | 7.97 | −47.3 | −25.5 | −21.8 |
| **3h** | 8.49 | −50.4 | −32.6 | −17.8 |
| **3i** | 7.80 | −46.3 | −24.3 | −22.0 |
| **3j** | 7.07 | −42.0 | −23.4 | −18.6 |
| **3k** | 7.86 | −46.7 | −26.4 | −20.3 |
| **3l** | 8.53 | −50.7 | −26.4 | −24.3 |
| **3m** | 8.47 | −50.3 | −31.8 | −18.5 |
| **3n** | 8.61 | −51.1 | −30.1 | −21.0 |
| **3o** | 8.05 | −47.8 | −27.6 | −20.2 |
| **3p** | 7.22 | −42.9 | −23.4 | −19.4 |
| **3q** | 8.61 | −51.1 | −29.3 | −21.8 |
| **3s** | 8.02 | −47.6 | −24.7 | −22.9 |
| **3t** | 7.83 | −46.5 | −26.0 | −20.5 |
| **3u** | 8.58 | −51.0 | −25.9 | −25.0 |
| **3v** | 7.69 | −45.7 | −26.0 | −19.7 |
| **3w** | 7.69 | −45.7 | −26.0 | −19.7 |
| **3x** | 8.26 | −49.0 | −25.5 | −23.5 |
| **3y** | 8.50 | −50.5 | −31.2 | −19.3 |
| **4c** | 9.96 (9.90) | −59.1 | −38.9 | −20.2 |
| **4e** | 10.20 | −60.6 | −39.3 | −21.3 |
| **4o** | 10.12 | −60.1 | −40.2 | −19.9 |

The standard error of the p$K_a$ determination was ±0.14. Thus the error of $\Delta_{b\_proton}G$ is ±0.94 kJ/mol. The standard error of enthalpy determination in ITC experiments was ±3.0 kJ/mol. Thus the summed error of the $T\Delta_{b\_proton}S$ is $\pm\sqrt{0.94^2 + 3.0^2} = \pm 3.14$ kJ/mol.

**Table 2**
Intrinsic thermodynamic parameters of 3 nonfluorinated and 3 fluorinated compound sulfonamide anion ($RSO_2NH^-$) binding to the protonated CA containing water molecule in the active site (CA–Zn-$H_2O$). Note that intrinsic $K_d$ for these extremely tightly binding compounds reach the affinity of 2 pM (**3e** with CA I). Affinities of fluorinated compounds are similar to non-fluorinated, a very different observation from the observed affinities where fluorinated compounds bind stronger by one to three orders of magnitude. Enthalpies and entropies vary significantly. ΔΔ shows the differences between fluorinated and non-fluorinated compounds.

| Protein | Parameter | **4c** | **3c** | $\Delta\Delta_{3c-4c}$ | **4e** | **3e** | $\Delta\Delta_{3e-4e}$ | **4o** | **3o** | $\Delta\Delta_{3o-4o}$ |
|---|---|---|---|---|---|---|---|---|---|---|
| CA I | $K_d$, nM | 0.15 | 0.011 | | 0.0029 | 0.0020 | | 0.0032 | 0.015 | |
| | $\Delta_bG$, kJ/mol | −58.3 | −65.1 | −6.8 | −68.5 | −69.4 | −0.9 | −68.3 | −64.2 | 4.0 |
| | $\Delta_bH$, kJ/mol | −55.7 | −84.0 | −28.3 | −62.9 | −74.4 | −11.5 | −57.5 | −62.0 | −4.5 |
| | $-T\Delta_bS$, kJ/mol | −2.6 | 18.9 | 21.5 | −5.6 | 5.0 | 10.6 | −10.7 | −2.2 | 8.5 |
| | $K_d$, nM | 0.084 | 0.34 | | 0.0070 | 0.062 | | 0.0040 | 0.063 | |
| CA II | $\Delta_bG$, kJ/mol | −59.8 | −56.2 | 3.6 | −66.1 | −60.6 | 5.5 | −67.6 | −60.6 | 7.1 |
| | $\Delta_bH$, kJ/mol | −55.2 | −51.1 | 4.1 | −69.0 | −46.4 | 22.6 | −58.3 | −40.7 | 17.6 |
| | $-T\Delta_bS$, kJ/mol | −4.7 | −5.2 | −0.5 | 2.9 | −14.2 | −17.1 | −9.3 | −19.9 | −10.6 |
| | $K_d$, nM | 0.090 | 0.55 | | 0.0097 | 0.028 | | 0.0050 | 0.026 | |
| CA VII | $\Delta_bG$, kJ/mol | −59.8 | −55.0 | 4.8 | −65.4 | −62.6 | 2.8 | −67.2 | −62.8 | 4.3 |
| | $\Delta_bH$, kJ/mol | −43.2 | −27.7 | 15.6 | −45.0 | −29.6 | 15.3 | −45.7 | −24.8 | 20.9 |
| | $-T\Delta_bS$, kJ/mol | −16.5 | −27.3 | −10.8 | −20.4 | −33.0 | −12.6 | −21.5 | −38.1 | −16.6 |
| | $K_d$, nM | 0.90 | 4.7 | | 0.067 | 1.2 | | 0.081 | 3.7 | |
| CA XII | $\Delta_bG$, kJ/mol | −53.7 | −49.4 | 4.3 | −60.4 | −53.1 | 7.3 | −59.9 | −50.1 | 9.8 |
| | $\Delta_bH$, kJ/mol | −41.5 | −33.8 | 7.7 | −56.4 | −31.7 | 24.7 | −52.0 | −30.8 | 21.1 |
| | $-T\Delta_bS$, kJ/mol | −12.2 | −15.7 | −3.5 | −4.0 | −21.4 | −17.4 | −8.0 | −19.3 | −11.3 |
| | $K_d$, nM | 1.4 | 0.68 | | 0.16 | 0.10 | | 0.034 | 0.017 | |
| CA XIII | $\Delta_bG$, kJ/mol | −52.5 | −54.4 | −1.9 | −58.1 | −59.4 | −1.3 | −62.1 | −64.0 | −1.9 |
| | $\Delta_bH$, kJ/mol | −39.6 | −54.3 | −14.7 | −47.6 | −54.3 | −6.8 | −55.5 | −47.9 | 7.5 |
| | $-T\Delta_bS$, kJ/mol | −13.0 | −0.1 | 12.8 | −10.6 | −5.1 | 5.5 | −6.7 | −16.1 | −9.4 |

benzenesulfonamides and the intrinsic binding thermodynamics toward five CA isoforms was determined.

## 2. Results and discussion

### 2.1. Thermodynamics of compound binding to CA

Binding thermodynamics of 25 inhibitors to five CA isoforms (CA I, CA II, CA VII, CA XII and CA XIII) was determined to enable detailed structure-energetics correlation analysis of such protein–ligand interactions. The chemical structures of fluorinated inhibitors of series **3** bearing various substituents at the *para* position (**a**–**y**) are shown in Fig. 1. Nonfluorinated inhibitors bearing hydroxyethylthio (**4c**), propylthio (**4e**) and phenylethylthio (**4o**) groups at the *para* position were also tested to reveal the contribution of fluorination on the thermodynamics of binding.

The binding of *para* substituted benzenesulfonamides to five CA isozymes was measured previously by FTSA [31]. In this work, we used ITC to examine the thermodynamics of binding of these ligands to five CA isoforms. ITC provides a more comprehensive thermodynamic description of the binding reaction, including the Gibbs free energy ($\Delta_bG_{obs}$), recalculated from the binding constant ($K_{b\_obs}$), the observed binding

**Table 3**
Intrinsic Gibbs free energies, enthalpies and entropies of the compound binding to human CA isoforms CA I, CA II, CA VII, CA XII and CA XIII at 37 °C (sulfonamide anion ($RSO_2NH^-$) binding to the protonated form of CA containing water molecule in the active site (CA–Zn-$H_2O$)).

| CA isoform | CA I | | | CAII | | | CA VII | | | CA XII | | | CA XIII | | |
|---|---|---|---|---|---|---|---|---|---|---|---|---|---|---|---|
| Compound | $\Delta G_{intr}$ | $\Delta H_{intr}$ (kJ/mol) | $-T\Delta S_{intr}$ | $\Delta G_{intr}$ | $\Delta H_{intr}$ (kJ/mol) | $-T\Delta S_{intr}$ | $\Delta G_{intr}$ | $\Delta H_{intr}$ (kJ/mol) | $-T\Delta S_{intr}$ | $\Delta G_{intr}$ | $\Delta H_{intr}$ (kJ/mol) | $-T\Delta S_{intr}$ | $\Delta G_{intr}$ | $\Delta H_{intr}$ (kJ/mol) | $-T\Delta S_{intr}$ |
| **1** | −58.7 | −72.6 | 13.9 | −54.1 | −43.0 | −11.1 | −57.1 | −23.2 | −33.8 | −48.2 | −32.0 | −16.1 | −53.3 | −41.3 | −12.0 |
| **2** | −58.4 | −69.2 | 10.8 | −53.7 | −41.2 | −12.6 | −55.9 | −20.2 | −35.7 | −46.6 | −30.7 | −15.9 | −51.0 | −39.3 | −11.7 |
| **3a** | −59.1 | −74.0 | 14.8 | −54.7 | −43.5 | −11.2 | −51.0 | −25.3 | −25.7 | −49.6 | −29.2 | −20.4 | −51.9 | −48.6 | −3.3 |
| **3c** | −65.1 | −84.0 | 18.9 | −56.2 | −51.1 | −5.2 | −55.0 | −27.7 | −27.3 | −49.4 | −33.8 | −15.7 | −54.4 | −54.3 | −0.1 |
| **3d** | −60.5 | −76.9 | 16.4 | −50.9 | −46.7 | −4.2 | −53.6 | −30.5 | −23.0 | −44.3 | −24.6 | −19.7 | −47.8 | −50.4 | 2.7 |
| **3e** | −69.4 | −74.4 | 5.0 | −60.6 | −46.4 | −14.2 | −62.6 | −29.6 | −33.0 | −53.1 | −31.7 | −21.4 | −59.4 | −54.3 | −5.1 |
| **3f** | −64.7 | −73.6 | 8.8 | −56.2 | −53.4 | −2.8 | −58.7 | −32.6 | −26.1 | −52.7 | −30.8 | −21.8 | −55.7 | −63.8 | 8.1 |
| **3g** | −62.0 | −80.4 | 18.4 | −53.7 | −55.7 | 2.0 | −56.0 | −32.2 | −23.8 | −50.2 | −25.7 | −24.4 | −52.0 | −54.3 | 2.4 |
| **3h** | −68.5 | −86.0 | 17.5 | −53.5 | −59.8 | 6.3 | −52.0 | −34.6 | −17.4 | −51.1 | −41.6 | −9.4 | −55.8 | −66.8 | 11.0 |
| **3i** | −64.0 | −60.3 | −3.7 | −57.0 | −42.2 | −14.7 | −57.9 | −30.9 | −27.0 | −53.2 | −35.2 | −18.0 | −57.8 | −42.3 | −15.4 |
| **3j** | −63.4 | −40.7 | −22.7 | −54.3 | −23.7 | −30.6 | −59.0 | −19.9 | −39.0 | −50.5 | −31.8 | −18.7 | −52.6 | −26.3 | −26.3 |
| **3k** | −65.0 | −77.6 | 12.5 | −58.5 | −57.8 | −0.7 | −61.4 | −24.5 | −36.9 | −51.1 | −39.8 | −11.4 | −59.1 | −43.9 | −15.3 |
| **3l** | −66.4 | −65.2 | −1.1 | −63.9 | −42.5 | −21.4 | −64.4 | −17.5 | −46.8 | −60.0 | −27.9 | −32.2 | −65.2 | −42.6 | −22.6 |
| **3m** | −66.6 | −76.4 | 9.8 | −58.5 | −55.6 | −2.9 | −52.1 | −26.2 | −25.9 | −49.6 | −39.5 | −10.1 | −58.3 | −51.6 | −6.8 |
| **3n** | −67.8 | −68.0 | 0.2 | −63.7 | −47.1 | −16.6 | −67.3 | −34.5 | −32.9 | −52.4 | −40.0 | −12.5 | −65.7 | −69.3 | 3.6 |
| **3o** | −64.2 | −62.0 | −2.2 | −60.5 | −40.7 | −19.9 | −62.8 | −24.8 | −38.1 | −50.1 | −30.8 | −19.3 | −64.0 | −47.9 | −16.1 |
| **3p** | −59.7 | −65.0 | 5.3 | −57.4 | −42.3 | −15.0 | −57.9 | −18.9 | −39.0 | −47.1 | −26.5 | −20.7 | −58.6 | −55.8 | −2.8 |
| **3q** | −68.5 | −84.7 | 16.2 | −57.6 | −51.9 | −5.6 | −54.1 | −39.9 | −14.2 | −49.4 | −45.0 | −4.4 | −55.0 | −49.2 | −5.8 |
| **3s** | −57.6 | −53.6 | −4.0 | −55.8 | −37.0 | −18.8 | −56.3 | −20.5 | −35.8 | −47.5 | −29.3 | −18.2 | −57.6 | −41.0 | −16.6 |
| **3t** | −58.7 | −53.0 | −5.6 | −60.4 | −37.7 | −22.8 | −65.1 | −27.5 | −37.6 | −47.4 | −31.9 | −15.5 | −62.5 | −43.7 | −18.9 |
| **3u** | −70.8 | −51.9 | −18.9 | −60.7 | −25.1 | −35.6 | −65.4 | −31.7 | −33.7 | −57.9 | −38.5 | −19.4 | −64.9 | −30.4 | −34.5 |
| **3v** | −60.6 | −54.7 | −5.9 | −55.1 | −35.1 | −20.0 | −54.0 | −21.4 | −32.6 | −48.2 | −33.5 | −14.8 | −55.9 | −43.7 | −12.2 |
| **3w** | −51.4 | −27.6 | −23.8 | −55.1 | −16.4 | −38.7 | −59.2 | −14.2 | −44.9 | −43.6 | −17.7 | −25.9 | −56.5 | −36.5 | −19.9 |
| **3x** | −70.3 | −59.7 | −10.6 | −56.5 | −45.5 | −11.0 | −56.7 | −25.7 | −30.9 | −51.5 | −31.8 | −19.7 | −54.8 | −35.6 | −19.2 |
| **3y** | −67.7 | −76.7 | 9.0 | −58.5 | −56.9 | −1.5 | −57.2 | −37.0 | −20.2 | −49.8 | −43.8 | −6.0 | −60.3 | −55.2 | −5.1 |
| **4c** | −58.3 | −55.7 | −2.6 | −59.8 | −55.2 | −4.7 | −59.8 | −43.2 | −16.5 | −53.7 | −41.5 | −12.2 | −52.5 | −39.6 | −13.0 |
| **4e** | −68.5 | −62.9 | −5.6 | −66.1 | −69.0 | 2.9 | −65.4 | −45.0 | −20.4 | −60.4 | −56.4 | −4.0 | −58.1 | −47.6 | −10.6 |
| **4o** | −68.3 | −57.5 | −10.7 | −67.6 | −58.3 | −9.3 | −67.2 | −45.7 | −21.5 | −59.9 | −52.0 | −8.0 | −62.1 | −55.5 | −6.7 |

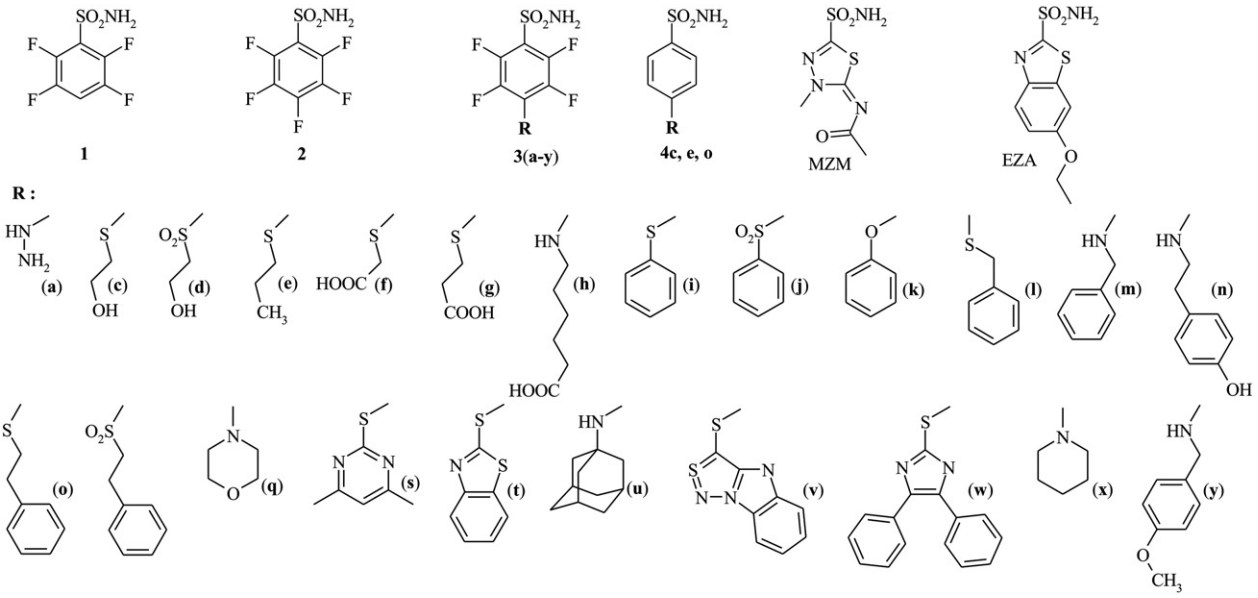


**Fig. 1.** Chemical formulas of compounds **1**, **2**, **3**(**a**, **c**–**q**, **s**–**y**) and **4**(**c**, **e**, **o**) used in this study. The numbers of most compounds are the same as in Ref. [31]. Methazolamide (MZM) and ethoxzolamide (EZA) were used as weak binders in ITC competition experiments.

enthalpy ($\Delta_bH_{obs}$) and entropy ($\Delta_bS_{obs}$). However, the main goal of this work is to determine the intrinsic Gibbs free energy ($\Delta_bG$), recalculated from intrinsic binding constant ($K_b$) or intrinsic dissociation constant ($K_d = 1/K_b$), intrinsic enthalpy ($\Delta_bH$) and intrinsic entropy ($\Delta_bS$). These intrinsic parameters were obtained after subtracting the linked protonation reactions.

Most of the fluorinated compound-bound CAs with $K_{d\_obs} < 1$ nM were too tight for direct observation by ITC because the Wiseman factor *c* was greater than 1000. However, the observed binding enthalpy could be accurately determined by ITC. We used displacement ITC [32] as well as a new calorimetric competition assay proposed by Keller et al. [33] to determine the $K_{d\_obs}$ for tight binding ligands and to confirm that $K_{d\_obs}$ values obtained by FTSA method were accurate. In a displacement experiment, a solution of a complex of CA I and low affinity ligand MZM, was titrated with the high affinity ligand **3e** (Fig. 2A). A competitive binding model was used to fit experimental data yielding $K_{d\_obs}$ = 40 pM and $\Delta_bH_{obs} = -56.3$ kJ/mol for **3e**. In a competition assay, the mixture of competing ligands, EZA and **3e**, was titrated by the protein (CA I) solution. The fitting of biphasic binding isotherm (Fig. 2B) yielded the thermodynamic parameters for the ligands, EZA and **3e**. The best-fit values for the thermodynamic parameters were $K_d$ = 36 nM and $\Delta_bH_{obs} = -32.2$ kJ/mol for EZA, as well as $K_d$ = 120 pM and $\Delta_bH_{obs} = -51.6$ kJ/mol for **3e**. The $K_d$ value for **3e** was about 3 times higher than obtained from FTSA method (33 pM) and displacement ITC (40 pM), but the latter two methods agree nearly perfectly.

The observed binding enthalpies for the same compound binding to five CAs differed significantly (Fig. 2C). In most cases, the binding of fluorinated compounds to CA I was the strongest and the observed enthalpy $\Delta_bH_{obs}$ the most favorable (−56.0 kJ/mol for **3e**, Fig. 2C).

The binding of benzenesulfonamide **4c** and its fluorinated analog **3c** to CA II became more exothermic with an increasing temperature (Fig. 2D). The change in heat capacity of binding for nonfluorinated ligand **4c** was −210 J/(mol × K), whereas for fluorinated analog **3c** −330 J/(mol × K). These negative $\Delta C_p$ values indicate hydrophobic interaction between the ligands and protein. The difference in the heat capacity of **3c** and **4c** is 120 J/(mol × K), and could be attributed to the larger hydrophobic surface area of **3c**. Whitesides group determined the difference in the heat capacity between fluorinated and nonfluorinated compounds to be equal to 184 J/(mol × K) [28]. However, the fluorines in their compounds were on the second ring relative to the sulfonamide group and thus direct comparison is not fully valid.

### 2.2. Thermodynamics of protonation of the sulfonamide and zinc-bound water molecule

The binding of sulfonamides to CAs is pH dependent, therefore the observed thermodynamic parameters depend on the fractions of both sulfonamide ligand and CA in their active forms [26,34]. In order to bind, sulfonamide must be deprotonated while the hydroxide bound to the active site Zn of CA must be protonated. To determine the intrinsic binding parameters and represent the binding of deprotonated sulfonamide to the protonated CA, the p$K_a$ and the enthalpies of ionization of protein and ligand must be determined.

The p$K_a$ of sulfonamide group for each compound was measured by the potentiometric titration of alkaline solution of benzenesulfonamides with HCl (Fig. 3A), or alternatively by measuring spectrophotometrically the absorption of compounds at different pHs (Fig. 3B).

All substituents of fluorinated benzenesulfonamides are bound to the *para* position of benzene ring through S, $SO_2$ or N atom. Compounds bearing substituents linked through $SO_2$ group (**3d**, **3j**, **3p**) had the lowest p$K_a$ (7.05–7.26), whereas the highest p$K_a$ values were observed for compounds with NH linker (for example, p$K_a$ of compounds **3a** and **3b** were 8.86 and 8.82, respectively). The p$K_a$ of two compounds with limited solubilities, **3l** and **3w**, were determined from the approximately linear correlation of NMR chemical shifts of protons of sulfonamide group with experimentally determined p$K_a$ (Fig. 3C). NMR spectra of fluorinated compounds including the $^1$H shifts have been described in [31].

The enthalpies of protonation ($\Delta_{b\_proton}H$) were measured for all compounds by ITC titration of the alkaline inhibitor solution with $HNO_3$ (Fig. 4). The enthalpies of protonation of nonfluorinated compounds were significantly more exothermic as compared to fluorinated compounds (Table 1). The measured p$K_a$ and $\Delta_{b\_proton}H$ for pentafluorobenzenesulfonamide **2** (8.1 and −26.4 kJ/mol, at 37 °C, respectively) were in good agreement with the literature (8.2 and −30.1 kJ/mol, at 25 °C) [34].

Furthermore, the enthalpies of compound protonation could be obtained by the van't Hoff relationship by determining the p$K_a$

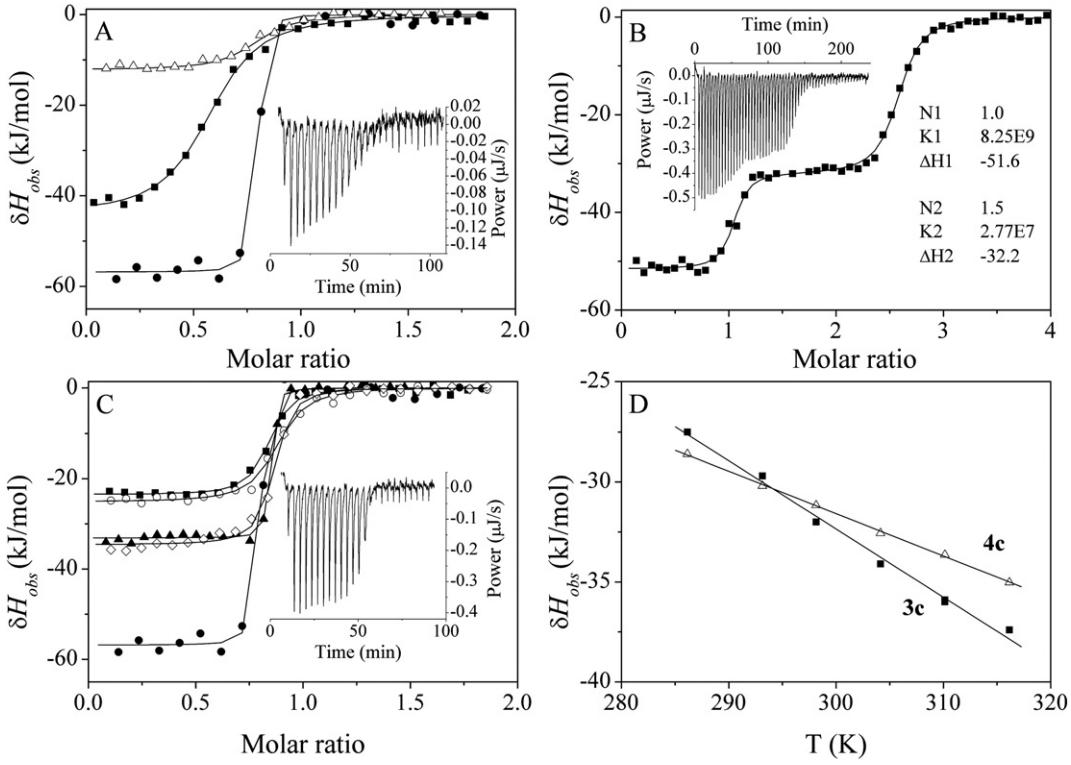


**Fig. 2.** Representative ITC data for the compound binding to CA. (A) Displacement ITC titration of the CA I pre-saturated with the weakly binding MZM by the tightly binding **3e** (Δ) (raw data in the inset). Direct ITC titrations of CA I with the tightly binding **3e** is shown as the steep curve (•) and the weakly binding MZM is shown by the middle curve (■). All three titrations were performed in 50 mM sodium phosphate, 100 mM NaCl, 1% DMSO, pH 7.0, 37 °C. (B) Competitive titration of EZA (7.5 μM in the cell) and **3e** (5 μM in the cell) with CA I (100 μM in the syringe), all in 50 mM sodium phosphate, 100 mM NaCl, 1% DMSO, pH 7.0, 37 °C. (C) Direct titration ITC data of **3e** binding to five CAs: CA I (•), CA XIII (◦), CA II (▲), CA XII (o) and CA VII (■). The inset shows raw data of **3e** binding to CA II. (D) Observed integral enthalpies of **3c** (■) and **4c** (Δ) binding to CA II as a function of temperature. The slopes of linear regression, representing the observed heat capacities of binding, were equal to −330 J/(mol × K) for **3c** and −210 J/(mol × K) for **4c**.

dependence on temperature. Fig. 3D shows the van't Hoff plots ($\ln K_a$ vs $T^{-1}$) for compounds **3e** and **3c**. The p$K_a$ decreased with increasing temperature. The values of $\Delta_{b\_proton}H$ calculated from the slopes of van't Hoff plots for **3e** and **3c** were −25.6 and −21.0 kJ/mol, respectively, close to the value determined by ITC (−26.4 kJ/mol) for both compounds.

Thermodynamic parameters of protonation of the hydroxide bound to the active center of five CA isoforms were previously determined [35]. Two isoforms, CA I and CA XIII, bearing the highest identity of amino acids in the active sites, had similar p$K_a$ (8.1 and 8.0, respectively, recalculated to 37 °C) and $\Delta_{b\_proton}H$ (−38.5 and −41.5 kJ/mol, respectively, at 37 °C), whereas p$K_a$ for CA II, CA VII and CA XII (6.9, 6.8 and 6.8, respectively, at 37 °C) and the enthalpies of protonation (−23.5, −25.5 and −30.5 kJ/mol, respectively, at 37 °C) were noticeably lower and less exothermic.

### 2.3. Compound structure correlations with intrinsic binding thermodynamics

Fig. 5 shows the intrinsic binding parameters of six compounds to five CA isoforms. The six compounds were selected to determine the effect of fluorination. Three compounds contain four fluorine atoms and a *para* substituent and other three compounds have the same *para* substituent but no fluorines on the benzene ring. The intrinsic $\Delta_bG$ (top number, bold), $\Delta_bH$ (middle number) and $T\Delta_bS$ (bottom number, italics) of binding are listed within the shapes and the values next to the arrows show the incremental differences in the thermodynamic values between the two compounds ($\Delta\Delta_bG$, $\Delta\Delta_bH$, $-T\Delta\Delta_bS$) which show how much binding energy is gained or lost when replacing a chemical group of the compound. Different colors on the map represent different CA isoforms, blue — CA I, yellow — CA XIII, green — CA II, red — CA VII, and black — CA XII. The order of the isozymes is shown according to the similarities of the active site of the proteins [35]. For example, CA I showed the greater similarity with CA XIII and CA VII (amino acid identities are 46.2%), whereas CA VII showed the closest similarity with CA II, CA XII and CA XIII (61.5%).

Ligands in the pair **4c**–**3c** exhibit very different changes in their thermodynamics of binding. Compound **3c** bound to CA I significantly more enthalpically than **4c** ($\Delta\Delta_bH_{\mathbf{4c-3c}} = -28.3$ kJ/mol, Table 2). Although the favorable enthalpy is partially compensated by the unfavorable entropy (enthalpy–entropy compensation), affinity upon fluorination increases ($\Delta\Delta_bG_{\mathbf{4c-3c}} = -6.8$ kJ/mol). Fluorination does not significantly change the binding affinity for the ligand pair **4e**–**3e** ($\Delta\Delta_bG_{\mathbf{4e-3e}} = -0.9$ kJ/mol) due to compensating changes in the binding enthalpy and entropy, whereas it decreases for the ligand pair **4o**–**3o** ($\Delta\Delta_bG_{\mathbf{4o-3o}} = 4.0$ kJ/mol). Fluorinated compounds **3c**,**e**,**o** bound to CA I with the larger exothermic enthalpy than their nonfluorinated analogs **4c**,**e**,**o**.

Fluorination of **4c**,**e**,**o** does not significantly change the binding affinity to CA XIII. However, the binding affinity increases when the *para* substituent becomes more hydrophobic. The lower affinity of the fluorinated compounds in comparison to the nonfluorinated ligands binding to CA II, CA VII and CA XII was mainly due to the smaller enthalpic contribution.

Comparing fluorinated vs non-fluorinated compound binding to all five CAs could be concluded that the fluorines significantly reduced the p$K_a$ of sulfonamide and therefore the observed $K_{b\_obs}$ was greater than for non-fluorinated compounds. However, the intrinsic $K_b$ was quite similar indicating that the recognition of fluorine atoms by the protein surface is quite similar to the recognition of hydrogens.

Fig. 6 compares the intrinsic binding parameters for all compound interaction with the five CA isoforms (Table 3). Compounds with similar structures are listed next to each other connected by arrows and the differences in the binding parameters are listed next to the arrows. Compound **1** (tetrafluorobenzenesulfonamide, in the center of Fig. 6) was one of the weakest binders. Addition of the fifth fluorine (**2**) did not

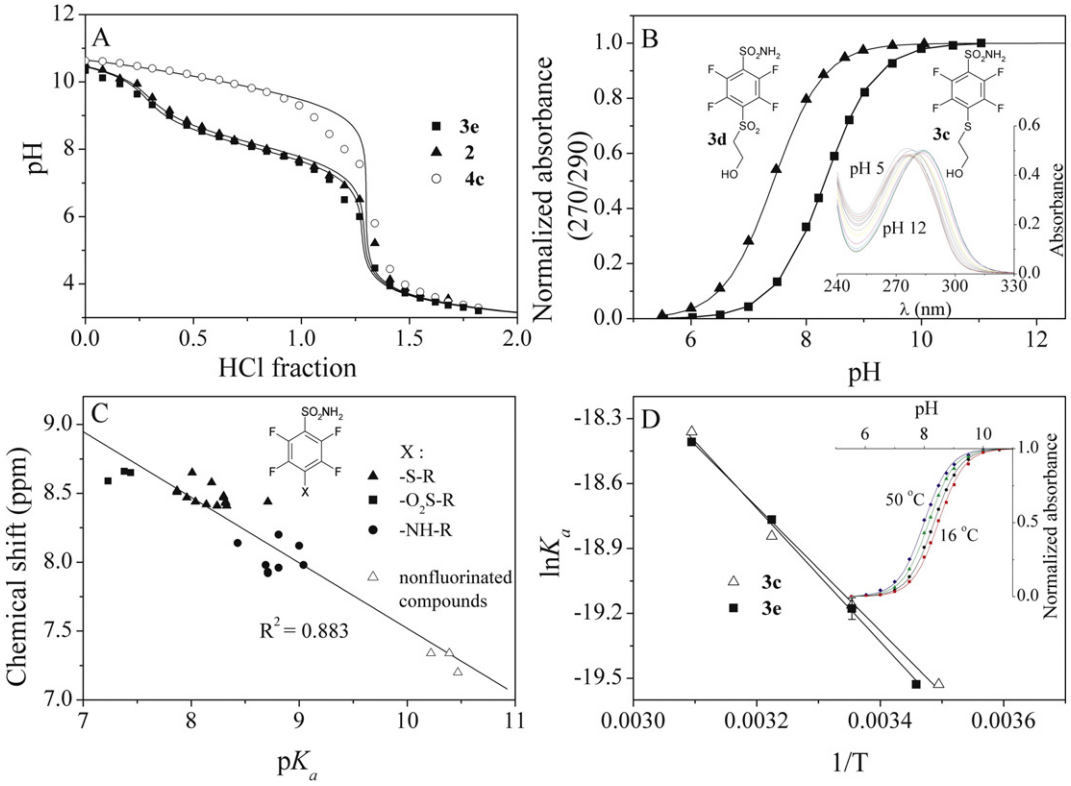


**Fig. 3.** Determination of the compound sulfonamide group protonation p$K_a$. (A) Potentiometric titration curves of compounds containing added 1.3 equivalent of NaOH. Two transitions are seen, one at 0.3 equivalent representing the reaction of $H^+$ with $OH^-$, and the protonation of one equivalent of sulfonamide. The p$K_a$ is approximately equal to the pH at the midpoint of the second stage of the titration. To determine the p$K_a$, the curves were fit to the standard pH titration model (solid lines). The p$K_a$ from potentiometric titration were equal to 8.05 for **3e** (■), 8.15 for **2** (▲) and 9.90 for **4c** (○), determined at 25 °C. (B) Spectrophotometric determination yielded the $pK_a$ values of 7.44 for **3d** (▲) and 8.32 for **3c** (■), at 25 °C. The inset shows the absorbance spectra of 50 μM **3c** at pH between 5.0 (blue line) and 12.0 (red line). (C) Approximately linear correlation between the p$K_a$ (determined by the spectrophotometric method) and the NMR chemical shift of the $NH_2$ group proton on the sulfonamide group. (D) The van't Hoff determination of the enthalpy of sulfonamide protonation by plotting ln$K_a$ vs 1/T for compounds **3e** (■) and **3c** (Δ). The insert shows normalized absorbance (ratio of $A_{270}/A_{290}$) for **3e** dependence on pH at temperatures from 16 °C (red line) to 50 °C (blue line).

significantly change any binding parameters. However, addition of the rigid piperidine ring in the *para* position (**3x**) significantly increased the binding affinity but reduced the exothermic contribution of the enthalpy, changing the entropic contribution from unfavorable to favorable. Therefore, it seems that **1** made better contacts with CA I than **3x**. The rigid piperidine ring reduced the ability of **3x** to make the same contacts as **1** thus reducing the enthalpy contribution. However this modification resulted in a moderate increase in binding affinity to other CAs (CA II, CA VII, CA XII and CA XIII, $\Delta\Delta_b G = -3.3 \div 0.4$ kJ/mol). The next modification to morpholine containing compound **3x** → **3q** caused a negligible impact to Gibbs free energy ($\Delta\Delta_b G = -1.1 \div 2.6$ kJ/mol) for all CAs, but these $\Delta\Delta_b G$ changes were hiding much larger changes in enthalpy and entropy to CA I binding ($\Delta\Delta_b H = -25.0$ kJ/mol, $-T\Delta_b S = 26.8$ kJ/mol) than to other CAs. Introduction of hydrophobic groups such as adamantylamino (**3u**) and benzylthio (**3l**) is mostly favorable for all CAs, but the enthalpy and entropy contributions to the binding affinity varied significantly. The Gibbs free energy for 25 fluorinated compound binding varied by $\Delta\Delta G = -13.1$ kJ/mol for CA II and by −16–19 kJ/mol for CA I, CA VII, CA XII and CA XIII.

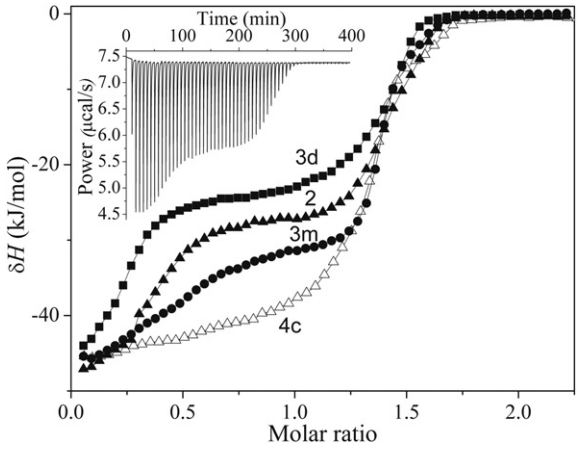


**Fig. 4.** Direct measurement of the sulfonamide protonation enthalpy as determined by ITC. The ITC data of **3d**, **2**, **3m** and **4c** in the cell (0.25 mM) containing 1.3 equivalents (0.325 mM) of added NaOH with 2.5 mM $HNO_3$ in the syringe at 37 °C. The inset shows the raw ITC data of **2**. The enthalpy of the second stage of the titration curve represents the enthalpy of sulfonamide protonation. The first stage of the titration curve represents the enthalpy of the reaction between $H^+$ and excess $OH^-$.

The enthalpy–entropy compensation graph for the six compounds binding to five CAs (Fig. 7A) shows that the affinities of the compounds span relatively narrow range ($\Delta\Delta_b G = -16.7$ kJ/mol) whereas enthalpies (−84.0–−24.8 kJ/mol) and entropies (−38.1–18.9 kJ/mol) span significantly wider ranges. Compounds exhibit strongly enthalpy-driven binding to all CAs, with the partial exception of CA VII where significant entropic contribution to the binding was observed.

Fig. 7B–F dissects the binding of each of the six compounds to the enthalpic and entropic contributions. Compounds are arranged pairwise to make fluorination contribution easily visible. In general, it reveals a dominant enthalpic contribution to the binding affinity. Binding of the fluorinated compounds to CA I and CA XIII becomes more enthalpically favorable than their nonfluorinated analogs and more entropically favorable as the *para* substituent becomes more hydrophobic. The enthalpy portion to the binding affinity of the fluorinated compounds to CA II,

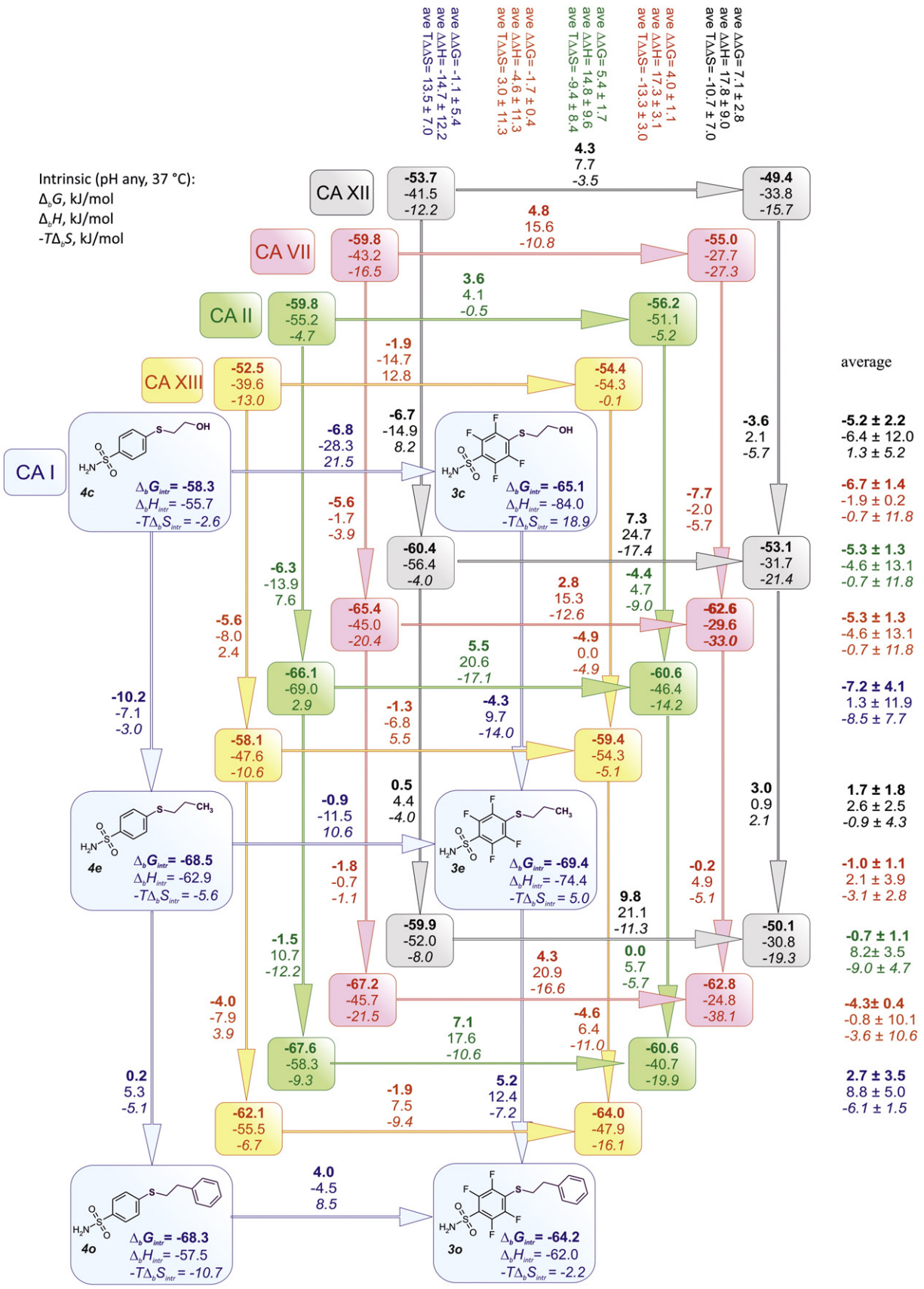


**Fig. 5.** Correlation map of the inhibitor chemical structures with the intrinsic thermodynamic binding parameters. Nonfluorinated compounds (left column) are compared with the fluorinated compounds (right column). Intrinsic parameters of binding are shown within shapes next to the chemical structures. Differences in the binding parameters between compounds are shown on the connecting arrows. Averages of the differences are listed on the top and right indicating the additivity of the parameters. Colors show different CA isoforms. Intrinsic Gibbs free energy values are shown in bold while the entropies are shown in italics.

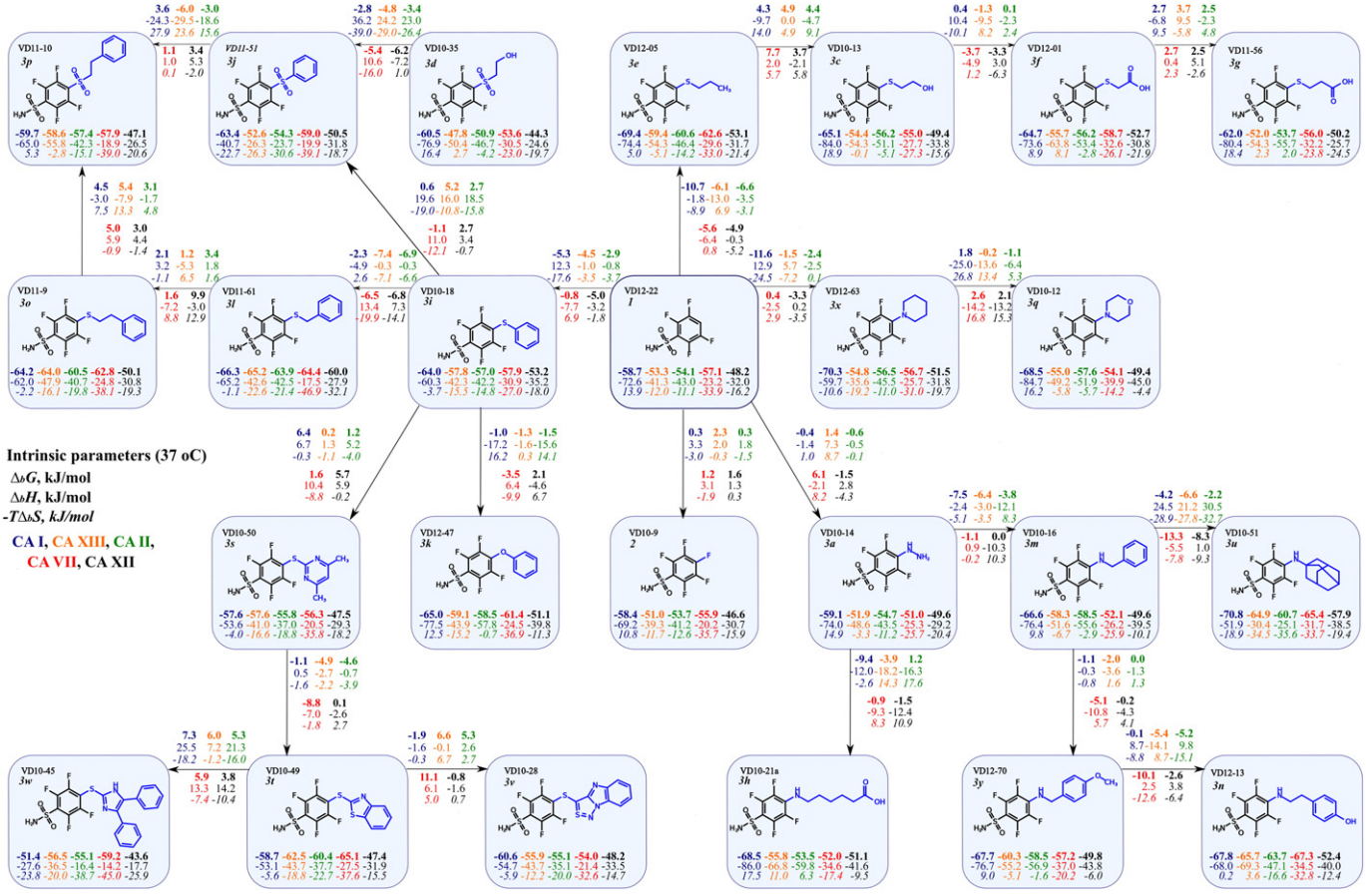


**Fig. 6.** The correlations of the fluorinated inhibitor chemical structures with the intrinsic thermodynamic parameters of binding to CA (37 °C). Intrinsic parameters of binding are shown within shapes below the chemical structures. Intrinsic Gibbs free energy values are shown in bold while the entropies are shown in italic. Differences in the binding parameters between adjacent compounds are shown on the connecting arrows. Colors show the different CA isoforms: CA I — blue, CA XIII — orange, CA II — green, CA VII — red and CA XII — black.

CA VII and CA XII is smaller than their nonfluorinated analogs. The increase in $\Delta_bG$ with increasing tail hydrophobicity going from hydroxyethylthio group in compounds **4c** and **3c** to methylethylthio group in **4e** and **3e** was observed for all tested CAs. The further increase of the substituent hydrophobicity to phenylethylthio group improved the binding affinity only for CA XIII. Interestingly, the replacement of the hydroxy group by the methyl group (**4c** → **4e** and **3c** → **3e**) and the latter replacement by the phenyl group (**4e** → **4o** and **3e** → **3o**) almost identically enhanced the Gibbs free energy of binding to CA XIII (average $\Delta\Delta_bG = -5.3$ and $-4.3$ kJ/mol, respectively).

The most clear feature in the binding thermodynamics of the majority of the compounds to CA I, is the strongly exothermic character, with negligible favorable or even unfavorable entropic contribution to the binding affinity. Unfavorable entropic contribution to the binding affinity was observable for 15 compounds binding to CA I, five compound containing hydrophilic groups (**3d**, **3g**, **3p**, **3h** and **3n**) binding to CA XIII and only two compounds (**3g** and **3h**) — to CA II. The entirely favorable enthalpic and entropic contributions were observed for CA VII and CA XII. Entropy contribution to the binding affinity toward CA VII is similar or even larger than enthalpy, completely distinct from CA I binding.

Fig. 8 lists compounds in the increasing order of their intrinsic Gibbs free energies of binding to each CA isoform (blue bars). Enthalpies are shown in green and entropies in red. Downward pointing contributions are favorable for the binding reaction to occur. CA VII clearly distinguishes itself as exhibiting a strong entropic contribution for most compounds, whereas CA I (Fig. 8A) has compounds that bound with the unfavorable entropy. There is no clear system in the order of the compounds, but some generalities could be observed. For example, compounds with the hydrophobic adamantyl group bound nearly strongest to all tested CAs.

It has been previously shown by the Whitesides group [29] that the hydrophobic substituents on the *para* position of benzenesulfonamides contribute favorably to the enthalpy and the entropy of binding. They proposed that the hydrophobic binding to the active site of CA II was due to the released water molecules that form stronger hydrogen bonds in bulk water — an enthalpically favorable process. Dehydration of the hydrophobic tail makes the dominant favorable contribution to the entropy. Our results are compatible with this finding. However, compounds with the hydrophilic groups (hydroxy, carboxy) bound to CA I in a different mode, the binding to CA I is clearly dominated by the favorable enthalpic contribution which is only partially compensated by the unfavorable entropy change.

### *2.4. Protein–compound crystallographic structure correlations with the intrinsic binding thermodynamics*

In order to determine the detailed structure–thermodynamics correlations, the crystal structures are needed for all protein–ligand complexes. In reality, however, structural characterization of the protein–ligand complex is not always feasible. However, if some crystal structures are available, they can significantly enhance our understanding of such protein–compound interactions.

Crystals of CA I with compounds **4c**, **3e** and **3x** were obtained by crystallization of pre-mixed complexes of inhibitors with the protein and yielded three crystal structures of CA I bound in the active site.

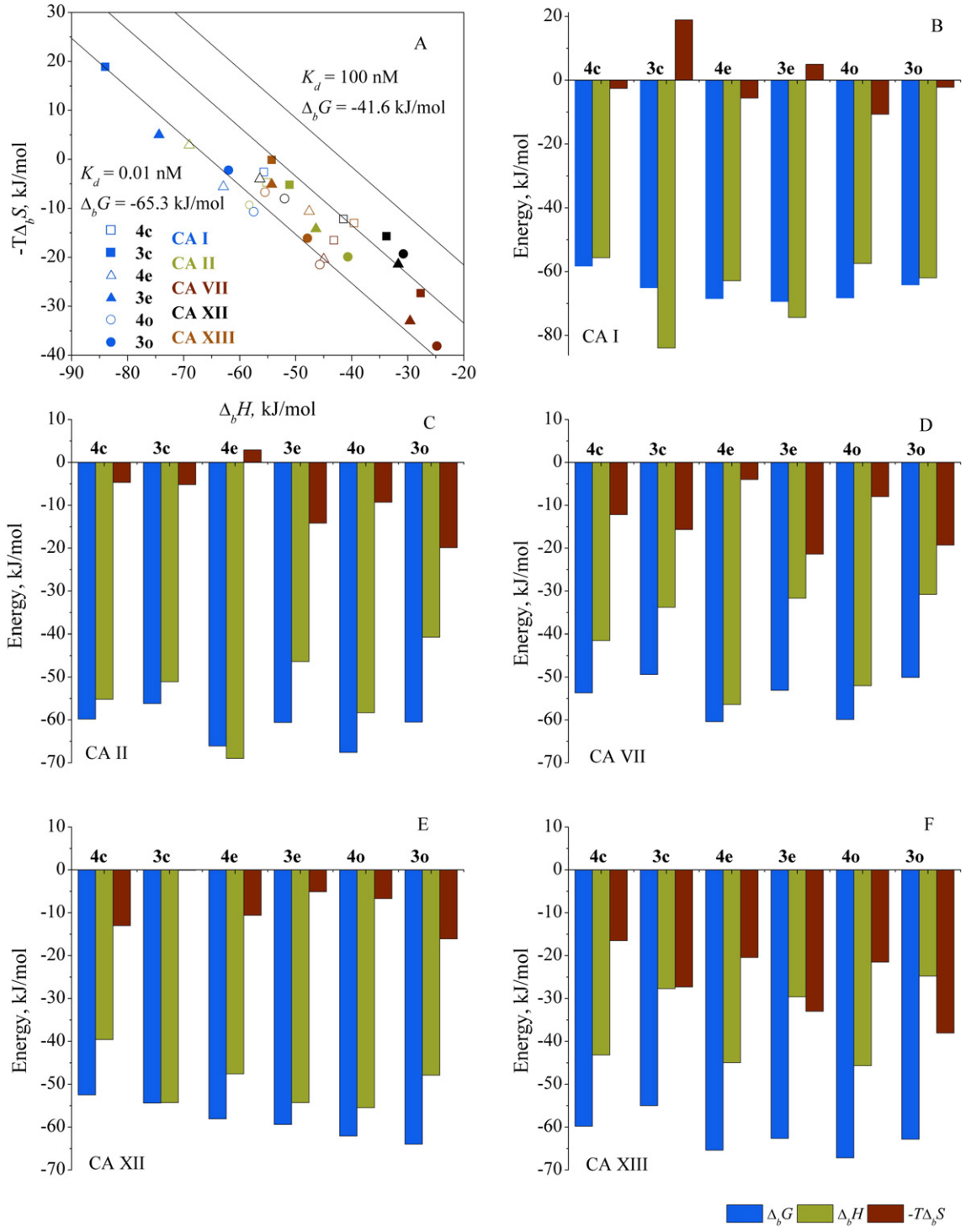


**Fig. 7.** Intrinsic thermodynamic parameters of compound binding to CAs: comparison between fluorinated and nonfluorinated compounds. (A) Enthalpy–entropy compensation graph. Filled symbols represent fluorinated compounds, open symbols — nonfluorinated compounds. Colors represent CA isozyme (CA I — blue, CA XIII — orange, CA II — green, CA VII — red and CA XII — black). Diagonal lines represent same affinities (100, 1.0 and 0.01 nM from top right to bottom left). Fluorinated compounds (filled symbols) have wider distribution of enthalpies and entropies than non-fluorinated compounds (open symbols). (B–F). The intrinsic thermodynamic parameters of binding shown as bars: $\Delta_b G$ (blue), $\Delta_b H$ (green), and $-T\Delta_b S$ (red). Nonfluorinated and fluorinated compound binding to CA I (B), CA II (C), CA VII (D), CA XII (E) and CA XIII (F). Favorable contributions point downwards while unfavorable upwards. The binding is enthalpy-driven for all CAs with smaller favorable entropy contribution, except for CA VII where the entropy contribution to the Gibbs free energy is similar to the enthalpy contribution.

Co-crystals of **4e** bound to CA XII and **3e** bound to CA II were obtained by soaking of the CA crystals with the corresponding ligand.

There were four protein chains in the asymmetric unit of CA XII crystals and two in the CA I crystals. The positions of ligands were essentially the same in all protein subunits within a crystal structure, except for the complex of **4c** in CA I, where the ligand was modeled in alternate conformation in the protein chain A. Fig. 9 shows the positions of ligands in the five crystal structures obtained in this study.

In the crystal structures of CA I and CA XII the benzene rings of all four compounds **4c**, **3e**, **4e** and **3x** were located in the same plane, along the O atom of the sulfonamide group (Fig. 9A, C, D and E). The benzene rings were located within 0.5–1.2 Å from each other. In

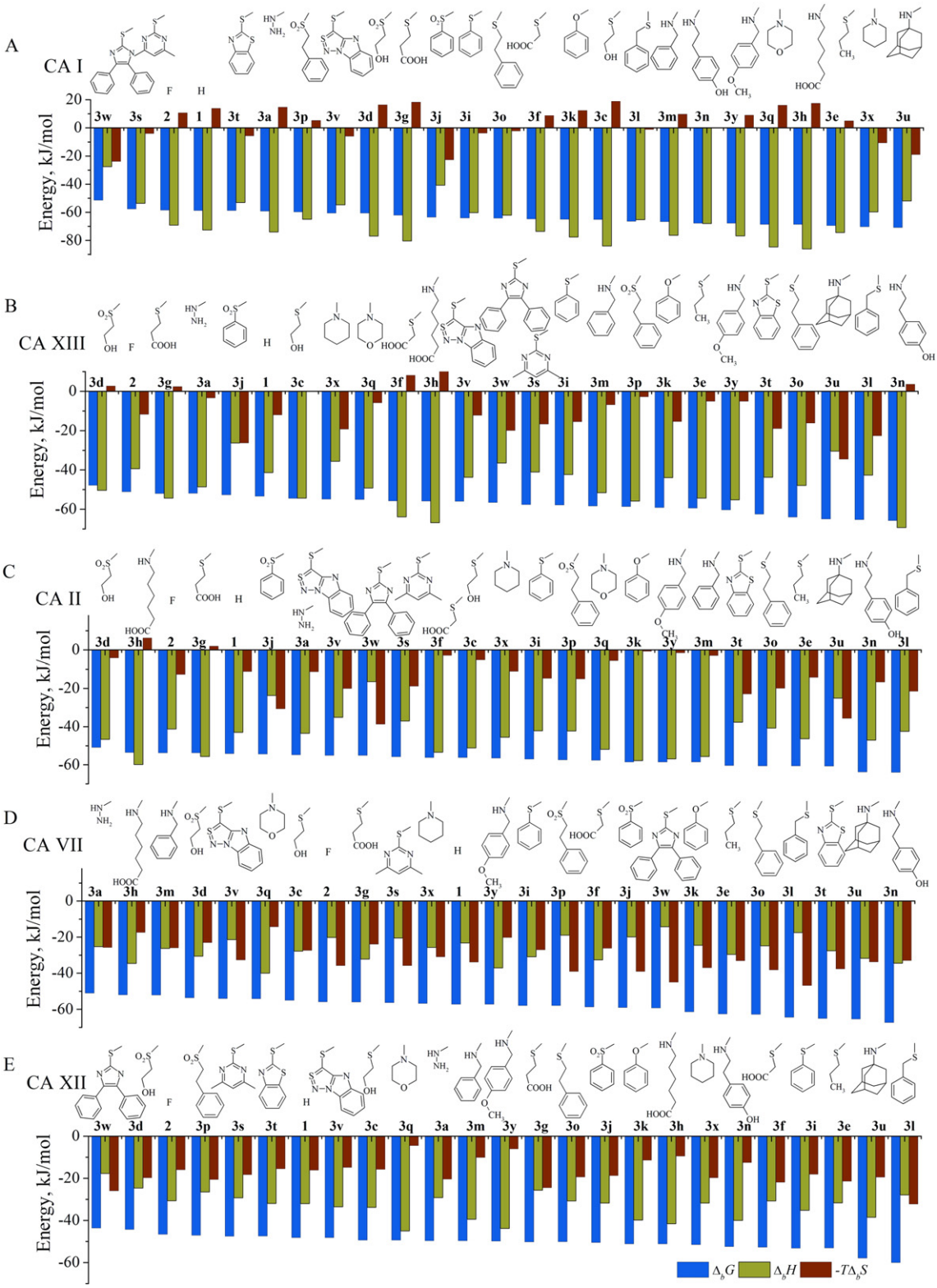


**Fig. 8.** Intrinsic thermodynamics of fluorinated compound binding to five CA isoforms: CA I (A), CA XIII (B), CA II (C), CA VII (D) and CA XII (E), arranged in the order of the similarity of their active sites. The chemical structures of compound R groups are shown on top of the bars. Compounds are arranged in the order of increasing intrinsic affinities ($\Delta_b G$, blue bars). Enthalpies are colored green while the entropies — red. Compound binding is mostly enthalpy-driven with the exception of CA VII and CA XII, where entropic component is also significant. However, some compounds, e.g. **3w**, have strong entropic contribution for all CAs.

contrast, **3e** bound to CA II had another orientation of the benzene ring, along the N atom of the sulfonamide group (Fig. 9B). The position of the fluorobenzene ring of **3e** and **3x** in complex with CA I was influenced by the histidine (His 200) which in other CAs is replaced by threonine (Thr199 in CA II and Thr200 in CA XII). The conformation of His200 in CA I was fixed by the hydrogen bond with the carbonyl oxygen of

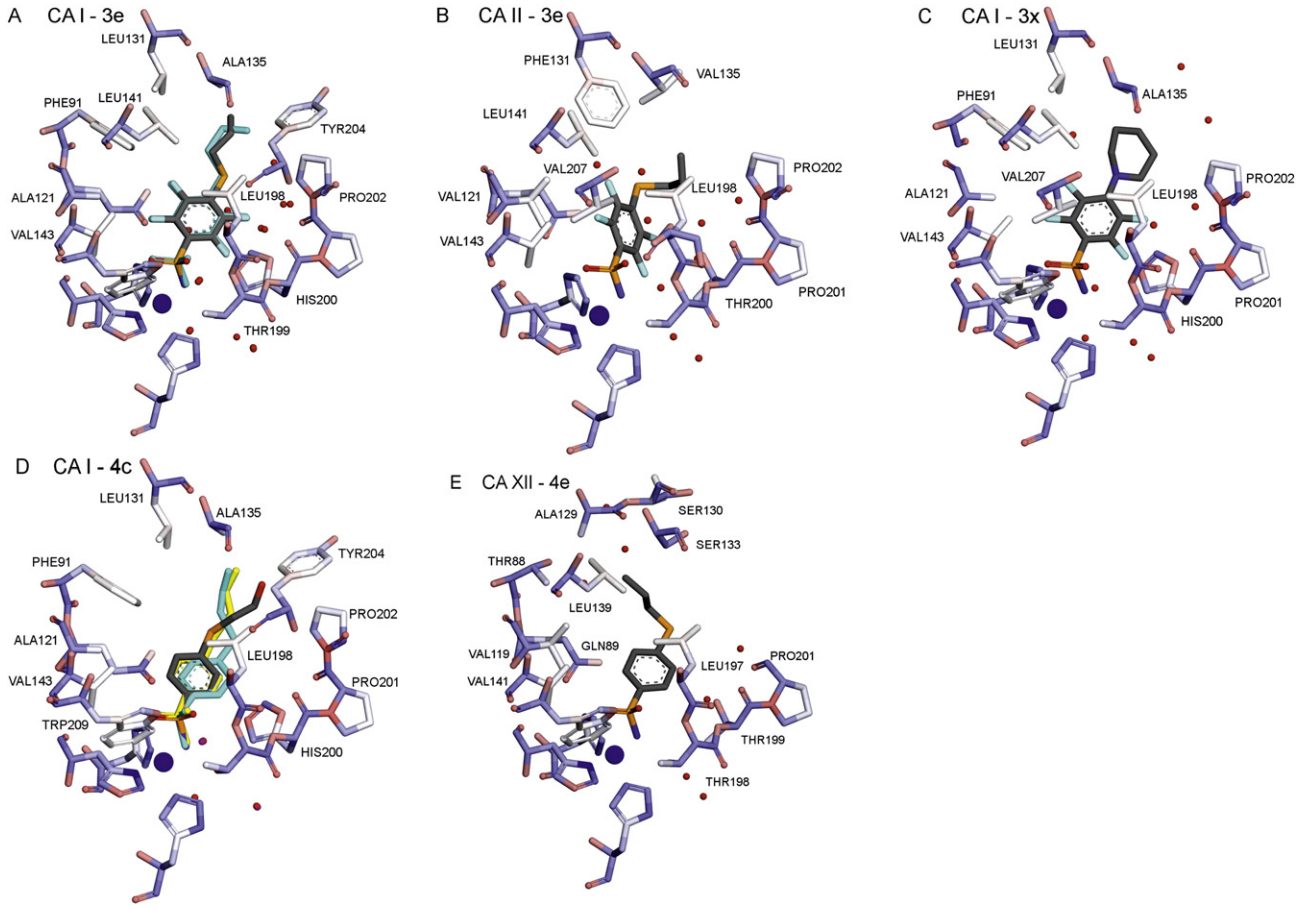


**Fig. 9.** The crystal structures of several compounds bound in the CA active site. (A) Compound **3e** bound to CA I (PDB ID: 4WR7). (B) Compound **3e** bound to CA II (PDB ID: 4WW6). (C) Compound **3x** bound to CA I (PDB ID: 4WUQ). (D) Compound **4c** bound to CA I (PDB ID: 4WUP). Two alternative conformations are seen of a flexible substituent group. (E) Compound **4e** bound to CA XII (PDB ID: 4WW8). The Zn atom is shown as a blue sphere, water molecules — as red spheres. Interacting protein amino acids (where the distance from the compound <5 Å) are shown. Compound sulfonamide amino group nitrogen makes a coordination bond with the Zn atom in each structure.

Pro201 and the atoms of His200 side-chain ring pushed on the fluorobenzene ring. The Leu198 restricted the fluorobenzene ring of the ligand from the other side (Fig. 9A, 12A).

Electron density maps of the compounds are shown in Fig. 10. The density was well resolved in all structures (Fig. 10A–C, F) except for **4c** bound to CA I where two conformations of the ligand could be modeled (Fig. 10D–E).

The comparison with the previously published crystal structures is shown in Fig. 11. In the crystal structures of CA II complexed with **3d** and **3s** [31] (4PZH and 4HT0, respectively), the fluorobenzene rings

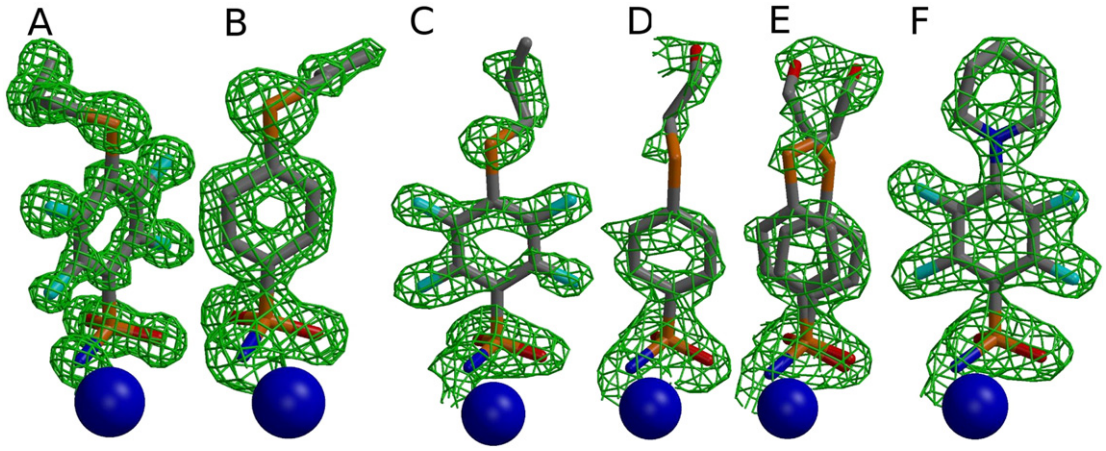


**Fig. 10.** Electron densities of compounds in the active centers of CAs: (A) **3e** in CA II contoured at 2.8σ, (B) **4e** in CA XII (protein chain A), contoured at 2.9σ, (C) **3e** in CA I (protein chain A), contoured at 2.7σ, (D) and (E) — **4c** in CA I, protein chains B and A, respectively, contoured at 2.7–2.5σ and (F) — **3x** in CA I (protein chain A), contoured at 2.7σ. Electron density maps $|F_{obs}–F_{calc}|$ were calculated in the absence of ligand. Zn atoms are shown as blue spheres.

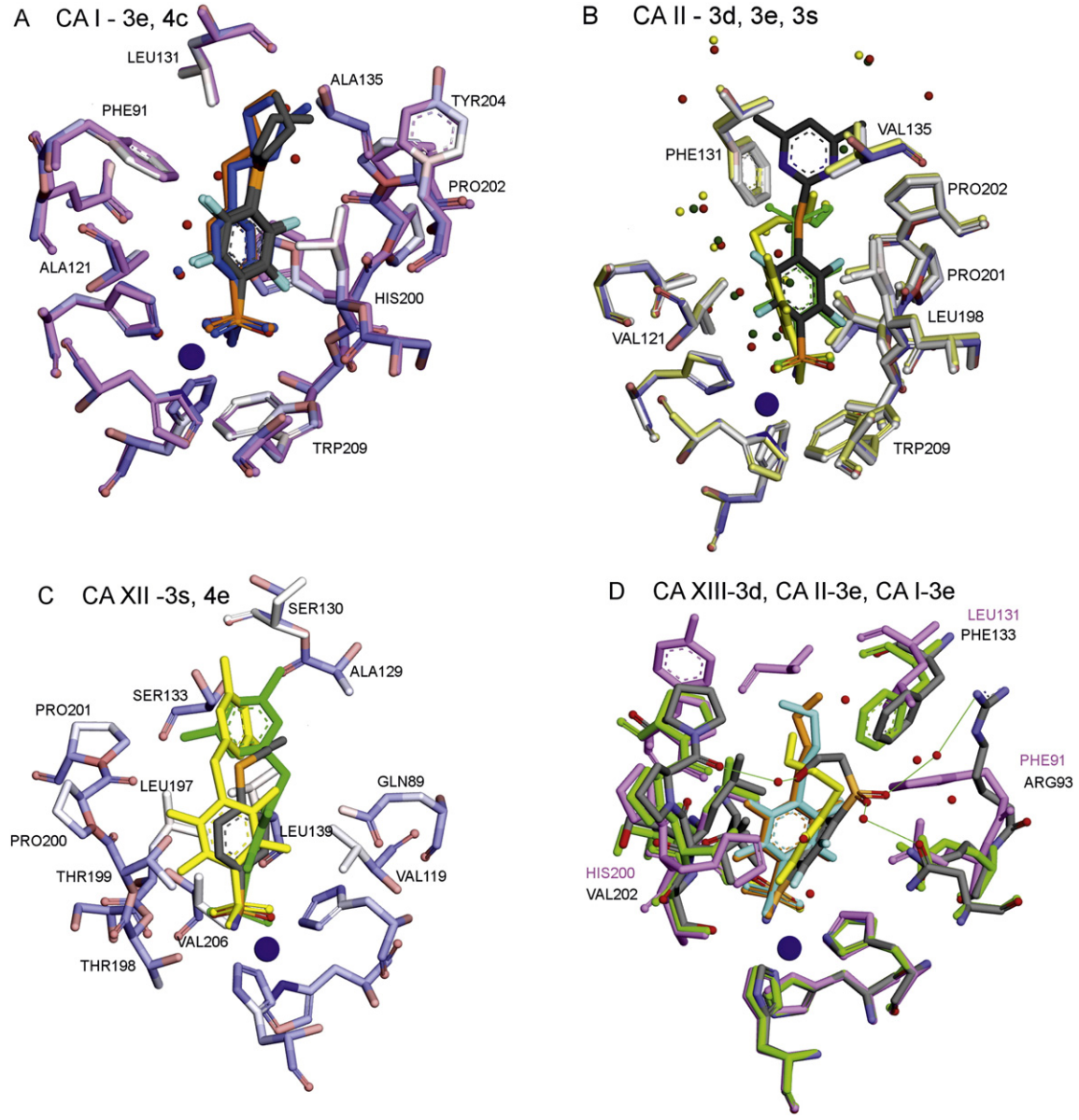


**Fig. 11.** Comparison of the binding modes of inhibitors in the active sites of CAs: (A) Compounds **3e** (gray) and **4c** (blue and orange) bound to CA I are located in the same plane, along the O atom of sulfonamide group. (B) Compound **3e** bound to CA II (yellow) exhibits a different rotated position of the benzene ring as compared to **3d** (green) and **3s** (dark gray). (C) In the complex of **3s** with CA XII (4HT2), the ligand (protein chain A) was found in two alternate positions (yellow and green), whereas **4e** exhibits only one position. (D) Comparison of positions of **3d** in CA XIII (colored gray, PDB ID 4HU1) with **3e** in CA I (**3e** is colored cyan and orange, CA I side chains are pink) and CA II (**3e** is yellow, CA II protein side chains are green). Hydrogen bonds between **3e**, water and side chains of CA XIII are shown as dotted lines.

were found in the same orientation as in the complexes of CA I with compounds **3e**, **3x** and **4c** (this study, Fig. 11A) in contrast to the crystal structure of **3e** in CA II (Fig. 11B). The same orientation as **3e** in complex with CA II was observed in the CA XIII complex with **3d** (4HU1) (Fig. 11D). In CA XII complex with **3s** (4HT2), the ligand bound in the protein chain A was also found in two alternate positions that represent both orientations of the fluorobenzene ring (Fig. 11C). In the other three subunits of this structure the fluorobenzene moiety is located in the same plane with the O atom of the sulfonamide group.

The changes in the entropy were generally unfavorable or negligible for CA I. For example, compounds **1** and **2**, bearing hydrogen and fluorine atom at the *para* position, respectively, exhibited positive $-T\Delta_bS$ values (13.9 and 10.8 kJ/mol, respectively). We speculate that the positive entropy changes for CA I reflect the single binding mode of fluorobenzene in CA I, where it is fixed between His200 and Leu198. The positive entropy change is also characteristic for binding of ligands with hydrophilic (amino, hydroxy and carboxy) groups to CA I. Compounds **3f**, **3g** and **3h** with the carboxy groups at the end of the *para* substituent, bound to CA I and CA XIII with the unfavorable entropy, opposite to the observations for CA II, CA VII and CA XII.

The hydrophobic propylthio group of **3e** in CA I and CA II and **4e** in CA XII oriented along the hydrophobic side chains (Phe131 in CA II and Leu131 in CA I) of the active sites. The interaction is hydrophobic. Piperidine group in **3x** occupied exactly the same position in CA I as the propyl of **3e** (Fig. 12A). Consequently, the binding affinities of **3e** and **3x** to CA I were the same (−69.4 and −70.3 kJ/mol, respectively).

The flexible propylthio (**4e**–**3e**) or hydroxyethylthio (**4c**–**3c**) groups can adopt any conformation near the hydrophobic side chains and are free to interact with the solution as it is the case with CA I bound **4c** (Fig. 10D–E, two alternate conformations were modeled). That means that the binding of **4c** is not uniform in the crystal. The thermodynamic values of the compound **4c** binding with CA I and **4e** with CA XII were

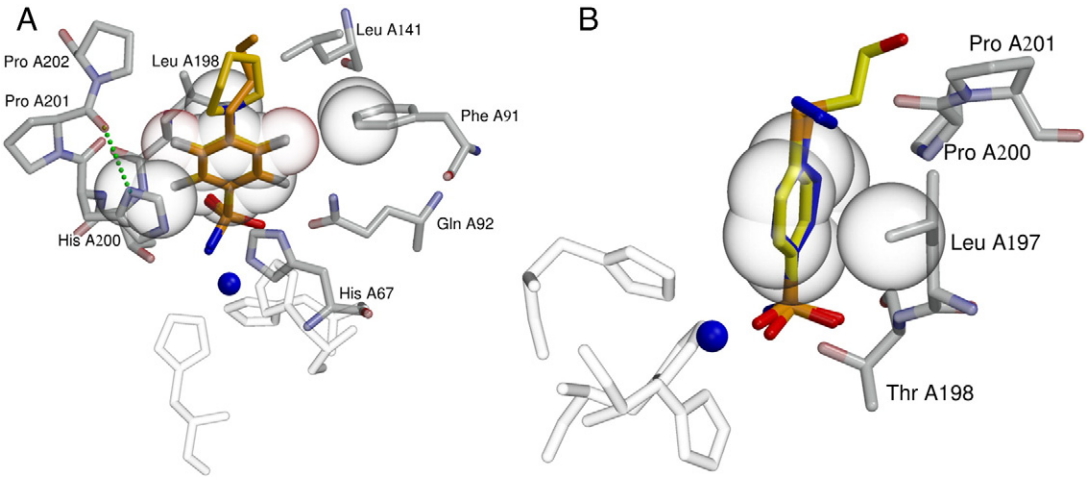


**Fig. 12.** Comparison of the position of fluorobenzene and benzene rings in the active sites of CA. (A) **3x** and **3e** in the active site of CA I. **3x** is colored yellow, **3e** — orange and the side chains of CA I (PDB ID 4WR7) — gray. His200, Leu198, fluorobenzene ring of **3e** and Phe91 are shown in CPK. The hydrogen bond between His200 and the main chain of Pro201 is shown as a dotted line. (B) Comparison of **4c** bound to CA I (one of two alternate conformations in chain A is shown in yellow) and **4e** in CA XII (blue). The labeled side chains of CA XII are shown in transparent gray. The benzene ring of **4e** and Leu197 are shown in CPK. Zn is shown as a blue sphere and the histidine residues complexing the Zn are transparent.

similar. The benzene ring of these compounds is located in similar position and tightly interacted with the side chain of leucine in both cases (Leu197 in CA XII, Leu198 in CA I). We speculate that similar thermodynamic profiles of **4c** binding to CA I ($\Delta_b G = -58.3$, $\Delta_b H = -55.7$, $-T\Delta_b S = -2.6$ kJ/mol) and **4e** binding to CA XII ($\Delta_b G = -60.4$, $\Delta_b H = -56.4$, $-T\Delta_b S = -4.0$) reflect the similar interactions of compounds with the identical amino acids of CAs (Fig. 12B).

## 3. Conclusions

Perfluorination of benzenesulfonamides containing the hydroxy-, methyl-, and phenylethylthio groups at the *para* position decreased the intrinsic binding affinity to CA II, CA VII and CA XII, whereas, for CA XIII, it did not change. The variation of the structure of only one substituent at the *para* position of the fluorinated benzenesulfonamide ring led to the compounds that bound CAs with the $K_d$ varying by 2 or 3 orders of magnitude with a broad range of enthalpy and entropy distributions. The fluorinated compounds bound CA I with a strongly exothermic enthalpy and a negligible favorable or unfavorable entropy change. CA VII had a larger entropy contribution to the binding affinity of most compounds than the enthalpy. Replacement of a single amino acid plays an important role in the positioning and tight fixing of the fluorobenzene ring in CAs. Fluorinated benzene ring has two positions in the crystal structures of CA II and CA XII, but only one in CA I — a possible reason or consequence of the exceptional affinity.

## 4. Materials and methods

### 4.1. Chemistry

The synthesis, chemical structural characterization, and the purity of 4-substituted-2,3,5,6-tetrafluorobenzenesulfonamides **3**(**a**, **c**–**q**, **s**–**y**) and 4-substituted-benzenesulfonamides **4**(**c**, **e**, **o**) has been previously described [31]. The synthesis and binding data of compounds **3x** and **3y** was described in Ref. [36] (the names in the manuscripts **8b** and **8a**, respectively). Instant JChem was used for structure database management, search and prediction, Instant JChem 6.1.3, 2013, ChemAxon (http://www.chemaxon.com).

### 4.2. Protein preparation

Production and purification of CAs I, II, VII, XII and XIII was performed as previously described: CA I in Ref. [37], CA II in [38], CAs VII and XIII in Ref. [39], and CA XII in Ref. [40].

### 4.3. Isothermal titration calorimetry

ITC experiments were performed using $ITC_{200}$ or VP-ITC instruments (Microcal, Inc., Northampton, USA, now part of Malvern Instruments Ltd., UK) with 5–20 μM protein solution in the cell and 50–200 μM of the ligand solution in the syringe. A typical experiment consisted of 18 or 25 injections (2 or 10 μl each) within 2 or 3–4 min intervals, respectively, for the two calorimeters. Experiments were carried out at 37 °C in a 50 mM sodium phosphate or TRIS chloride buffer containing 100 mM NaCl at pH 7.0, with a final DMSO concentration of 1–2%, equal in the cell and syringe. Protein stock solutions were dialyzed against the buffers that were used to prepare the ligand solutions. ITC data were analyzed using MicroCal Origin software. The first point from the 1–3 μL injection in the integrated data graph was deleted. The binding constants, enthalpies and entropies of binding were estimated after fitting the data with the single binding site model.

To determine the $K_{b\_obs}$ values of high affinity ligands, the displacement ITC was used where CA I was pre-saturated with a marginally binding ligand (methazolamide, MZM) and the ligand was displaced by titration with the stronger one. The results of these experiments were analyzed according to the method proposed by Sigurskjold [32].

The $K_{b\_obs}$ of high affinity ligands were also measured by the competition assay described by Krainer [33]. The solution containing two inhibitors, 5 μM of high affinity ligand and 7.5 μM of the weak ligand (ethoxzolamide, EZA), were titrated by 100 μM CA I. Automated baseline assignment and peak integration were accomplished by use of NITPIC [41]. Data analysis was performed with software SEDPHAT [42] or Origin 7.

The enthalpy of inhibitor deprotonation was measured using VP-ITC instrument. Inhibitor (0.25 mM) was deprotonated by adding 1.3 equivalent of NaOH and titrated with 2.5 mM $HNO_3$. A typical experiment consisted of 58 injections (5 μl each) added at 4 min intervals. Experiments were performed at 37 °C with the final DMSO concentration of 0.5%, equal in the syringe and the sample cell.

**Table 4**
Crystallization conditions, X-ray crystallographic data collection and the refinement statistics. All datasets were collected at 100 K, test set size was 10%.

| PDB ID | 4WUP | 4WR7 | 4WUQ | 4WW6 | 4WW8 |
|---|---|---|---|---|---|
| Compound | **4c** | **3e** | **3x** | **3e** | **4e** |
| CA isoform | CA I | CA I | CA I | CA II | CA XII |
| Crystallization buffer | 0.1 M Tris–HCl (pH 8.5), 0.2 M ammonium acetate and 24% PEG4000 | 0.1 M Tris–HCl (pH 8.5), 0.2 M sodium acetate (pH 8.3), 28% PEG3350 | 0.1 M HEPES sodium (pH 7.5), 0.2 M ammonium sulfate and 24% PEG4000 | 0.1 M sodium BICINE (pH 9.0), 0.2 M ammonium sulfate and 2 M sodium malonate (pH 7.0) | 0.1 M ammonium citrate (pH 7.0), 0.2 M ammonium sulfate and 30% PEG4000 |
| Spacegroup | $P2_12_12_1$ | $P2_12_12_1$ | $P2_12_12_1$ | $P12_11$ | $P12_11$ |
| Unit cell Å | a = 63.33, b = 71.28, c = 120.72, α = β = γ = 90° | a = 62.35, b = 72.03, c = 121.11, α = β = γ = 90° | a = 62.60 b = 71.20, c = 119.94 α = β = γ = 90° | a = 42.21, b = 41.03, c = 71.77, α = γ = 90°, β = 104.29 | a = 77.31, b = 74.26, c = 91.57, α = γ = 90°, β = 108.66 |
| Resolution (Å) | 1.75 (71.28) | 1.50 (121.11) | 1.75 (119.93) | 1.06 (69.55) | 1.42 (74.26) |
| $N_{ref}$ (unique) | 733336 (55864) | 85187 (1093283) | 726651 (54897) | 676004 (102717) | 1192219 (176873) |
| $R_{merge}$, (outer shell) | 0.085 (0.345) | 0.064 (0.374) | 0.073 (0.411) | 0.041 (0.350) | 0.054 (0.370) |
| $I/\sigma$ (outer shell) | 16.6 (6.3) | 17.0 (4.2) | 21.4 (7.3) | 17.9 (4.1) | 16.7 (3.9) |
| Multiplicity (outer shell) | 13.1 (13.2) | 12.8 (9.9) | 13.2 (13.4) | 6.6 (5.8) | 6.7 (5.6) |
| Completeness (%) (outer shell) | 100.0 (100.0) | 96.8 (79.1) | 100.0 (100.0) | 95.4 (83.0) | 95.8 (79.0) |
| $N_{atoms}$ | 4517 | 4744 | 4525 | 2585 | 9594 |
| $R_{work}$ | 0.185 | 0.195 | 0.173 | 0.128 | 0.172 |
| $R_{free}$ | 0.232 | 0.232 | 0.210 | 0.151 | 0.205 |
| $B_{average}$ | 24.6 | 20.9 | 21.5 | 15.3 | 18.5 |
| $RMS_{bonds}$ | 0.020 | 0.023 | 0.022 | 0.024 | 0.024 |
| $RMS_{angles}$ | 2.012 | 2.368 | 2.099 | 2.417 | 2.270 |

### 4.4. Determination of sulfonamide protonation $pK_a$

Compound solution (0.5–1.0 mM, containing 2% DMSO and 0.75–1.5 mM NaOH (1.5 added equivalent to fully deprotonate the sulfonamide group)) was titrated with 10–20 mM HCl (containing 2% DMSO). Titration was performed with the VP-ITC calorimeter syringe held outside the calorimeter while stirring and measuring pH with a microelectrode (Mettler Toledo). Forty four injections of 10 μl HCl were made (every 60 s) into 2.5 ml of the sulfonamide inhibitor solution, at 25 °C.

To determine the $pK_a$ of the ligands we also used the procedure described by Snyder [30]. Ligand solution (final concentration 12.5–100 μM, containing 1% DMSO) was added to a buffer solution (100 mM, ranging from pH 5.5 to 12.5 at every half pH unit) and a UV–VIS spectra were recorded at 25 °C. The ratio of absorbances (typically 10 nm above and below the isosbestic point) was plotted as a function of pH. The $pK_a$ value was determined by the fitting of the curve. The $pK_a$ values determined at 25 °C were recalculated to 37 °C by using van't Hoff equation. The van't Hoff enthalpies were determined (to be compared to the enthalpies obtained by ITC) by determining the $pK_a$ spectrophotometrically at various temperatures (16, 25, 37 and 50 °C).

### 4.5. Intrinsic thermodynamics

The observed binding constants and observed enthalpies are dependent on the experimental conditions (buffer components and pH). The intrinsic binding constant $K_b$ is equal to the observed binding constant $K_{b\_obs}$ divided by the available fractions of deprotonated inhibitor and protonated zinc hydroxide anion (water molecule):

$$K_b = \frac{K_{b\_obs}}{\left(f_{RSO_2NH^-}\, f_{CAZnH_2O}\right)}. \tag{1}$$

The fractions of the deprotonated inhibitor and the CA in water form can be calculated if both $pK_a$ values are known:

$$f_{RSO_2NH^-} = \frac{10^{pH-pK_{a\_sulf}}}{1 + 10^{pH-pK_{a\_sulf}}} \tag{2}$$

$$f_{CAZnH_2O} = 1 - \frac{10^{pH-pK_{a\_ZnH_2O}}}{1 + 10^{pH-pK_{a\_ZnH_2O}}}. \tag{3}$$

The observed enthalpy is the sum of all protonation events and the binding reaction. Linked reactions that have to be subtracted are the protonation/deprotonation of buffer, deprotonation of sulfonamide, and the protonation of the hydroxide anion bound to active site zinc:

$$\Delta_b H = \Delta_b H_{obs} - n_{sulf}\Delta_{b\_proton\_sulf}H - n_{CA}\Delta_{b\_proton\_CA}H + n_{buf}\Delta_{b\_proton\_buf}H\,. \tag{4}$$

where $\Delta_b H_{obs}$ is the observed binding enthalpy, $n_{sulf} = f_{RSO_2NH^-} 1$ is the number of protons binding to the inhibitor, $\Delta_{b\_proton\_sulf}H$ is the enthalpy of inhibitor protonation, $n_{CA} = 1 - f_{CAZnH_2O}$ is the number of protons bound to the Zn-hydroxide, $\Delta_{b\_proton\_CA}H$ is the enthalpy of CA protonation, $n_{buf} = n_{sulf} + n_{CA}$, is the net sum of uptaken or released protons and $\Delta_{b\_proton\_buf}H$ is the buffer protonation enthalpy. The enthalpy of Tris protonation is equal to −46.56 kJ/mol and the enthalpy of phosphate buffer protonation is equal to −2.876 kJ/mol at 37 °C [43].

### 4.6. Crystallization

Co-crystals of CA II and CA XII with the inhibitors were obtained by soaking of the CA crystals in the crystallization buffer supplied with 0.5 mM inhibitor. Diffraction data from the soaked crystals were collected after several days. Crystal structures of CA I with inhibitors were obtained by crystallizing CA I (28.3–52 mg/ml) containing 0.6–1.0 mM

inhibitor because the crystals of the apoprotein did not survive the soaking procedure.

### 4.7. Data collection and structure determination

X-ray diffraction datasets were collected at the EMBL macromolecular crystallography beam lines P13 and P14 at PETRAIII storage ring, DESY, Hamburg (Germany). The X-ray diffraction datasets were collected at the macromolecular crystallography beam lines P13 and P14 at EMBL Hamburg. Data collection and the refinement statistics are presented in Table 4. All datasets were processed by XDS [44]. MOLREP [45] was used for molecular replacement. The protein chain of PDB entry 1JD0 was chosen for the phasing of CA XII, 1CAB for CA I and 3HLJ for CA II. 3D models of inhibitors were created using molecule editor AVOGADRO [46]. The chemical and geometrical descriptions of the inhibitors used in the refinement were generated by LIBCHECK [47]. REFMAC [48] was used for model refinement. COOT [49] was used for model rebuilding.

## Acknowledgments

This research was funded by the European Social Fund under the Global Grant measure (no. VP1-3.1.-SMM-07-K-02-009). The authors thank the local contacts at the EMBL beamlines Dr. G. Bourenkov and Dr. M. Cianci for the help with P13 and P14 EMBL beamline operations at PETRAIII storage ring (DESY, Hamburg).

## References

[1] J.E. Ladbury, G. Klebe, E. Freire, Adding calorimetric data to decision making in lead discovery: a hot tip, Nat. Rev. Drug Discov. 9 (2010) 23–27.
[2] J.D. Chodera, D.L. Mobley, Entropy–enthalpy compensation: role and ramifications in biomolecular ligand recognition and design, Annu. Rev. Biophys. 42 (2013) 121–142.
[3] J. Gomez, E. Freire, Thermodynamic mapping of the inhibitor site of the aspartic protease endothiapepsin, J. Mol. Biol. 252 (1995) 337–350.
[4] V.M. Krishnamurthy, B.R. Bohall, V. Semetey, G.M. Whitesides, The paradoxical thermodynamic basis for the interaction of ethylene glycol, glycine, and sarcosine chains with bovine carbonic anhydrase II: an unexpected manifestation of enthalpy/entropy compensation, J. Am. Chem. Soc. 128 (2006) 5802–5812.
[5] T.S.G. Olsson, J.E. Ladbury, W.R. Pitt, M.A. Williams, Extent of enthalpy–entropy compensation in protein–ligand interactions, Protein Sci. 20 (2011) 1607–1618.
[6] K. Sharp, Entropy–enthalpy compensation: fact or artifact? Protein Sci. 10 (2001) 661–667.
[7] V. Lafont, et al., Compensating enthalpic and entropic changes hinder binding affinity optimization, Chem. Biol. Drug Des. 69 (2007) 413–422.
[8] J.B. Chaires, Calorimetry and thermodynamics in drug design, Annu. Rev. Biophys. 37 (2008) 135–151.
[9] E. Freire, Isothermal titration calorimetry: controlling binding forces in lead optimization, Drug Discov. Today Technol. 1 (2004) 295–299.
[10] E. Freire, The thermodynamic linkage between protein structure, stability, and function, Methods Mol. Biol. 168 (2001) 37–68.
[11] G.A. Holdgate, Making cool drugs hot: isothermal titration calorimetry as a tool to study binding energetics, Biotechniques 31 (2001) 164–166 (168, 170).
[12] A. Biela, M. Betz, A. Heine, G. Klebe, Water makes the difference: rearrangement of water solvation layer triggers non-additivity of functional group contributions in protein–ligand binding, ChemMedChem 7 (2012) 1423–1434.
[13] A. Biela, et al., Dissecting the hydrophobic effect on the molecular level: the role of water, enthalpy, and entropy in ligand binding to thermolysin, Angew. Chem. Int. Ed. Engl. 52 (2013) 1822–1828.
[14] B. Breiten, et al., Water networks contribute to enthalpy/entropy compensation in protein–ligand binding, J. Am. Chem. Soc. 135 (2013) 15579–15584.
[15] S.W. Homans, Water, water everywhere — except where it matters? Drug Discov. Today 12 (2007) 534–539.
[16] G. Klebe, Applying thermodynamic profiling in lead finding and optimization, Nat. Rev. Drug Discov. 14 (2015) 95–110.
[17] S.G. Krimmer, M. Betz, A. Heine, G. Klebe, Methyl, ethyl, propyl, butyl: futile but not for water, as the correlation of structure and thermodynamic signature shows in a congeneric series of thermolysin inhibitors, ChemMedChem 9 (2014) 833–846.
[18] B.M. Baker, K.P. Murphy, Evaluation of linked protonation effects in protein binding reactions using isothermal titration calorimetry, Biophys. J. 71 (4) (1996) 2049–2055.
[19] H. Zhao, P. Schuck, Global multi-method analysis of affinities and cooperativity in complex systems of macromolecular interactions, Anal. Chem. 84 (2012) 9513–9519.
[20] C.T. Supuran, Carbonic anhydrases: novel therapeutic applications for inhibitors and activators, Nat. Rev. Drug Discov. 7 (2008) 168–181.
[21] C.T. Supuran, Carbonic anhydrases — an overview, Curr. Pharm. Des. 14 (2008) 603–614.
[22] M. Aggarwal, B. Kondeti, R. McKenna, Insights towards sulfonamide drug specificity in α-carbonic anhydrases, Bioorg. Med. Chem. 21 (2013) 1526–1533.
[23] M. Aggarwal, C.D. Boone, B. Kondeti, R. McKenna, Structural annotation of human carbonic anhydrases, J. Enzyme Inhib. Med. Chem. 28 (2013) 267–277.
[24] M.I. Hassan, B. Shajee, A. Waheed, F. Ahmad, W.S. Sly, Structure, function and applications of carbonic anhydrase isozymes, Bioorg. Med. Chem. 21 (2013) 1570–1582.
[25] S. Lindskog, Structure and mechanism of carbonic anhydrase, Pharmacol. Ther. 74 (1997) 1–20.
[26] V.M. Krishnamurthy, et al., Carbonic anhydrase as a model for biophysical and physical-organic studies of proteins and protein–ligand binding, Chem. Rev. 108 (2008) 946–1051.
[27] S.Z. Fisher, M. Aggarwal, A.Y. Kovalevsky, D.N. Silverman, R. McKenna, Neutron diffraction of acetazolamide-bound human carbonic anhydrase II reveals atomic details of drug binding, J. Am. Chem. Soc. 134 (2012) 14726–14729.
[28] M.R. Lockett, et al., The binding of benzoarylsulfonamide ligands to human carbonic anhydrase is insensitive to formal fluorination of the ligand, Angew. Chem. Int. Ed. Engl. 52 (2013) 7714–7717.
[29] J. Mecinović, et al., Fluoroalkyl and alkyl chains have similar hydrophobicities in binding to the "hydrophobic wall" of carbonic anhydrase, J. Am. Chem. Soc. 133 (2011) 14017–14026.
[30] P.W. Snyder, et al., Mechanism of the hydrophobic effect in the biomolecular recognition of arylsulfonamides by carbonic anhydrase, Proc. Natl. Acad. Sci. U. S. A. 108 (2011) 17889–17894.
[31] V. Dudutienė, et al., 4-Substituted-2,3,5,6-tetrafluorobenzenesulfonamides as inhibitors of carbonic anhydrases I, II, VII, XII, and XIII, Bioorg. Med. Chem. 21 (2013) 2093–2106.
[32] B.W. Sigurskjold, Exact analysis of competition ligand binding by displacement isothermal titration calorimetry, Anal. Biochem. 277 (2000) 260–266.
[33] G. Krainer, J. Broecker, C. Vargas, J. Fanghänel, S. Keller, Quantifying high-affinity binding of hydrophobic ligands by isothermal titration calorimetry, Anal. Chem. 84 (2012) 10715–10722.
[34] V.M. Krishnamurthy, et al., Thermodynamic parameters for the association of fluorinated benzenesulfonamides with bovine carbonic anhydrase II, Chem. Asian. J. 2 (2007) 94–105.
[35] M. Kišonaitė, et al., Intrinsic thermodynamics and structure correlation of benzenesulfonamides with a pyrimidine moiety binding to carbonic anhydrases I, II, VII, XII, and XIII, PLoS One 9 (2014) e114106.
[36] V. Dudutienė, et al., Functionalization of fluorinated benzenesulfonamides and their inhibitory properties toward carbonic anhydrases, ChemMedChem 10 (2015) 662–687.
[37] E. Čapkauskaitė, et al., Benzenesulfonamides with pyrimidine moiety as inhibitors of human carbonic anhydrases I, II, VI, VII, XII, and XIII, Bioorg. Med. Chem. 21 (2013) 6937–6947.
[38] P. Cimmperman, et al., A quantitative model of thermal stabilization and destabilization of proteins by ligands, Biophys. J. 95 (2008) 3222–3231.
[39] J. Sūdžius, et al., 4-[N-(substituted 4-pyrimidinyl)amino]benzenesulfonamides as inhibitors of carbonic anhydrase isozymes I, II, VII, and XIII, Bioorg. Med. Chem. 18 (2010) 7413–7421.
[40] V. Jogaitė, et al., Characterization of human carbonic anhydrase XII stability and inhibitor binding, Bioorg. Med. Chem. 21 (2013) 1431–1436.
[41] S. Keller, et al., High-precision isothermal titration calorimetry with automated peak-shape analysis, Anal. Chem. 84 (2012) 5066–5073.
[42] J.C.D. Houtman, et al., Studying multisite binary and ternary protein interactions by global analysis of isothermal titration calorimetry data in SEDPHAT: application to adaptor protein complexes in cell signaling, Protein Sci. 16 (2007) 30–42.
[43] J.J. Christensen, L.D. Hansen, R.M. Izatt, Handbook of proton ionizations heats, Wiley-Interscience, 1976.
[44] W. Kabsch, XDS, Acta Crystallogr. D Biol. Crystallogr. 66 (2010) 125–132.
[45] A. Vagin, A. Teplyakov, MOLREP: an automated program for molecular replacement, J. Appl. Crystallogr. 30 (1997) 1022–1025.
[46] M.D. Hanwell, et al., Avogadro: an advanced semantic chemical editor, visualization, and analysis platform, J. Cheminform. 4 (2012) 17.
[47] CCP4 (Collaborative Computational Project, N. 4), The CCP4 suite: programs for protein crystallography, Acta Crystallogr. D 50 (1994) 760–763.
[48] G.N. Murshudov, A.A. Vagin, E.J. Dodson, Refinement of macromolecular structures by the maximum-likelihood method, Acta Crystallogr. D Biol. Crystallogr. 53 (1997) 240–255.
[49] P. Emsley, K. Cowtan, Coot: model-building tools for molecular graphics, Acta Crystallogr. D Biol. Crystallogr. 60 (2004) 2126–2132.